e-Prime - Advances in Electrical Engineering, Electronics and Energy 6 (2023) 100368

Contents lists available at ScienceDirect

e-Prime - Advances in Electrical Engineering, Electronics and Energy

journal homepage: www.elsevier.com/locate/prime

Design of an elliptically-slotted patch antenna for multi-purpose wireless wi-Fi and biosensing applications

Jeena George, Mfonobong Uko *, Sunday Ekpo, Fanuel Elias

Manchester Metropolitan University, United Kingdom

ARTICLE INFO

Keywords:
5G
Biosensor
Elliptically-slotted patch antenna
Gain
IoT
Wireless communication

ABSTRACT

Radio frequency (RF) biosensor research is advancing in the medical point-of-care diagnostics field with the increased demand for smart adaptive contactless RF biosensors for a holistic tailored healthcare provisioning including cancer detection. This paper introduces an elliptically-slotted patch antenna (ESPA) designed to perform optimally in biosensing applications. The verified performance shows resonance frequency difference of the ESPA is 2.5% compared with the primary slot-less patch antenna of 6.6%. Hence, the proposed model compares with the conventional slot-less patch antenna, demonstrating a significant improvement in its bandwidth efficiency by over 62%. The fabricated ESPA yields a total gain of 6.75 dBi at 2.74 GHz. This novel biosensing antenna is suitable for bio-sample detection and signal transmission applications. Moreover, the reported novel ESPA will support multipurpose sub-6 GHz 5G/Wi-Fi 6/6E (2.4 GHz, 5 GHz, and 6 GHz) point-of-care diagnostics wireless data transmission and connectivity for medical applications. This system's miniaturised size enhances a compact, portable label-free, reliable, real-time detection with a cost-effective fabrication. The highly sensitive ESPA satisfies the minimum size, weight and power-to-cost (SWaP-C) requirements.

1. Introduction

In the rapidly evolving landscape of wireless communications, there is a growing demand for multifunctional devices capable of serving varied applications while conserving space and providing optimal performance [1]. A critical component in the arena of wireless communication systems is the antenna, a device responsible for transmitting and receiving electromagnetic waves [2]. The development and integration of compact, efficient, and broadband antennas are essential to ensure the robustness and versatility of modern communication systems [3,4].

Patch antennas have emerged as a preferred choice for many wireless applications due to their low-profile, ease of fabrication, and compatibility with integrated circuits. Traditional rectangular and circular patch antennas have long been the focus of research and have found widespread applications in Wi-Fi, satellite communication, and various other wireless systems [5–7]. However, the need for antennas with broader bandwidth, dual-band or multi-band operation, and unique radiation characteristics has spurred research into more complex geometries and configurations [8,9].

Slot antennas have been utilized in many different applications and provide a number of benefits. Different antenna slot designs are examined, and they offer the further benefit of allowing for required bandwidth modifications [10]. In order to function in the sub-6 GHz 5G bandwidth of 2.32 GHz-5.24 GHz, an ultra-wideband antenna based on a redesigned ground plane is provided [11]. It has also been suggested to use elliptical/circular slots [12], T-shaped slots [13], L-shaped slots [14], and numerous other forms of the slots incorporated in the antenna geometry targeting multiband operation [15]. The elliptically-slotted patch antenna is one of these novel designs that has gained popularity. In today's diversified wireless environment, their unique structure makes it possible for them to have expanded bandwidth and several resonant frequencies [16]. Specifically, the incorporation of elliptical slots in the patch not only provides a means to introduce multi-band operation but also offers an opportunity to tailor the radiation patterns to cancer detection and bio-sensing applications.

Furthermore, with the growing interest in the field of bio-sensing, where antennas play a pivotal role in sensing biological parameters and ensuring communication between sensors and devices, the need for multifunctional antennas has never been greater. The capability of elliptically-slotted patch antennas to operate at frequencies relevant to both Wi-Fi communication and biosensing applications can lead to groundbreaking advancements in integrated wireless health monitoring

* Corresponding author.
E-mail address: mfonuko12@gmail.com (M. Uko).

https://doi.org/10.1016/j.prime.2023.100368
Received 19 September 2023; Received in revised form 10 November 2023; Accepted 21 November 2023
Available online 2 December 2023

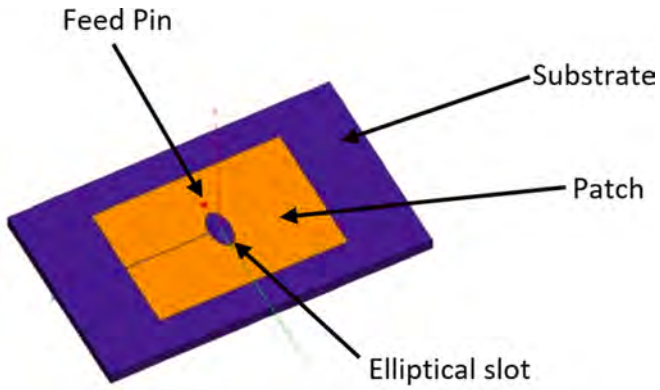

Fig. 1. ESPA System on Finite Ground.

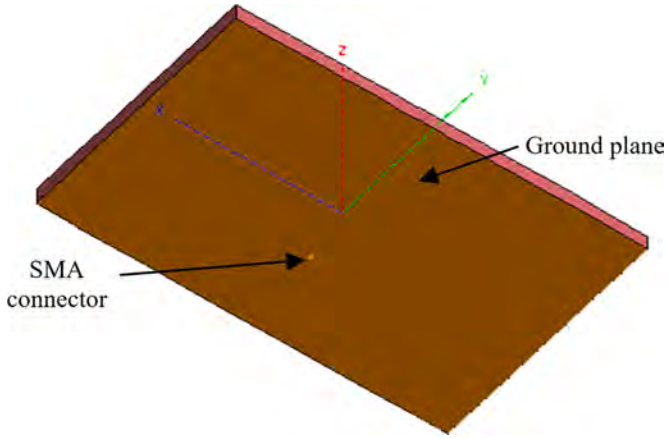

Fig. 2. ESPA System (Back View).

systems [17]. For instance, the use of radio waves and intense magnetic fields to identify the variation in energy absorption rate birthed the magnetic resonance imaging (MRI) technique. This method enhances picture quality with the introduction of contrast liquid into breast tissues and is excellent at late-stage cancer cells diagnosis [18]. Existing literatures have shown lower values of permittivity and conductivity for fatty tissues and higher values for the glandular tissues with the breast tissue [19]. With the assistance of its electrical property variations, radio waves can detect the existence of small malignant tissues in a rapid, sensitive and specific way. Due to the emission of non-ionising radiation, patients favour microwave-based breast imaging methods. This method considers the variation in the electrical properties (such as permittivity and conductivity) of each tissue, depending on the water content of the tissues. These properties are exploited to detect tumour presence from the healthy host tissue, as malignant tissues possess more water and thereby higher permittivity than other tissues [2,20]. The return loss (S_{11}) and the dielectric properties corresponding to each biotic specimen varies under RF/microwave frequencies, and antenna biosensors exploit this feature for sensing.

The proposed first-order ESPA design yields a total gain of 6.75 dBi at 2.74 GHz. With a digitally assisted reconfigurable nth-order ESPA, very low resonance frequency differences would be achieved at the respective resonant frequencies for the infinite approximation and the finite substrate. This would enable the sub-6 GHz Wi-Fi 6E bands (including 2.4 GHz, 5 GHz, and 6 GHz) to be realised on-demand. Its functional significance is in the seamless connectivity of the growing number of devices in the world. The potential high directivity of the proposed ESPA design promises to enhance 5G-enabled point-of-care diagnostics and other vertical use cases applications. Moreover, a frequency shift due to the fringing fields around a patch antenna makes it seem longer. Consequently, the general design rule-of-thumb is to trim a conventional patch antenna by typically 2–4% to enable it to resonate at the desired centre-design frequency. The presented novel ESPA obviates the need for an undue antenna sizing by optimising its elliptically slotted fractals to account for the potential fringing fields near its radiating surface.

This paper is organised as follows. Section II presents the elliptically-

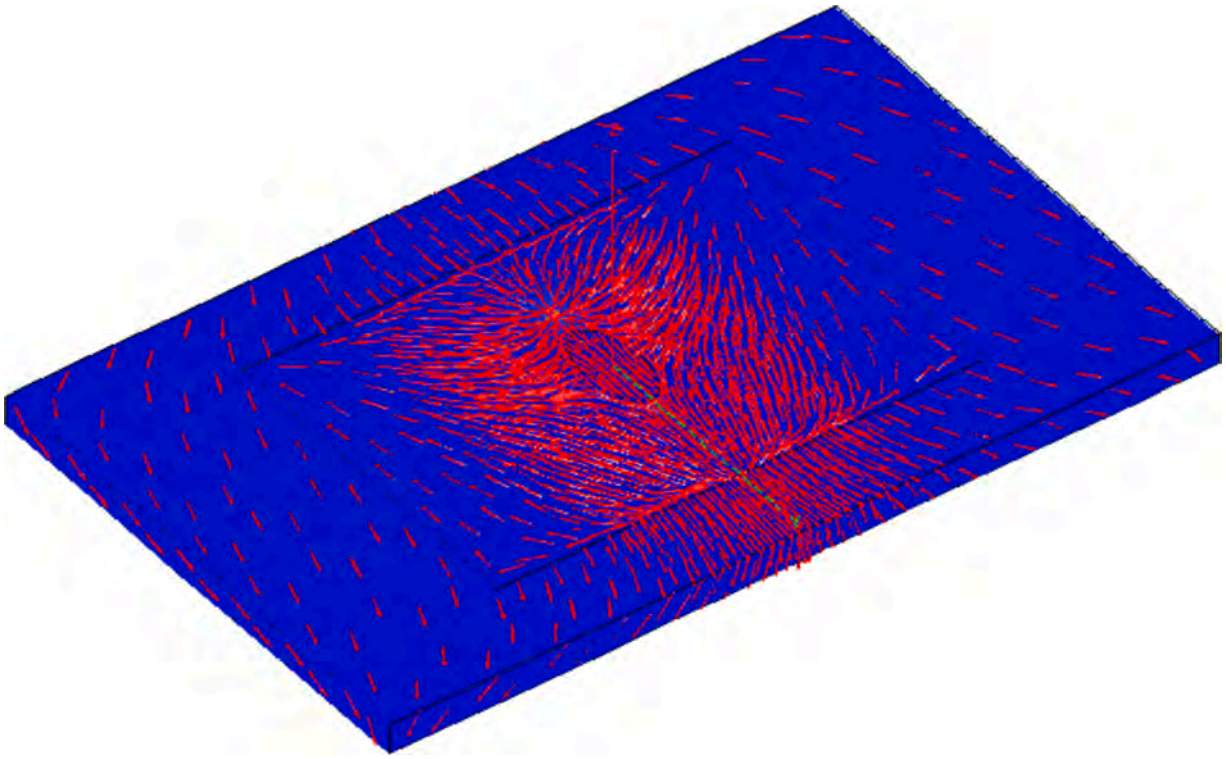

Fig. 3. Instantaneous Electric Field Current of the ESPA Model.

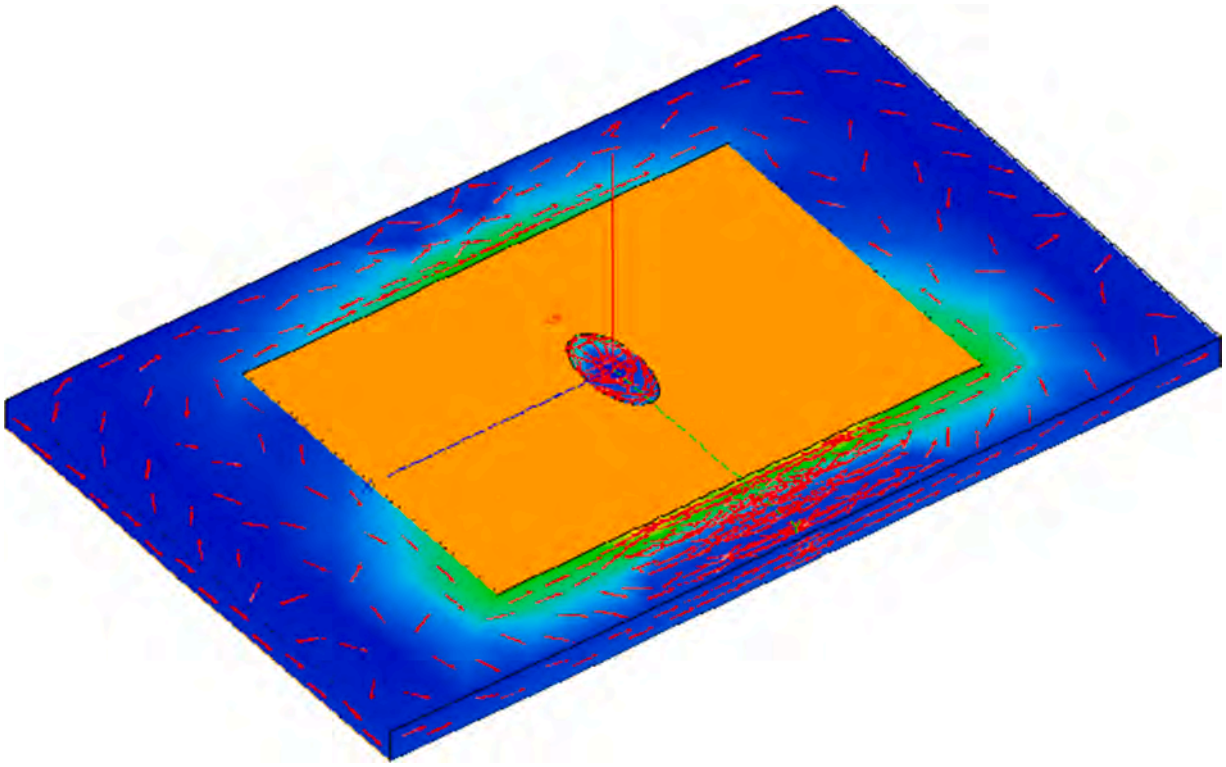

Fig. 4. Instantaneous Magnetic Field Current of the ESPA Model.

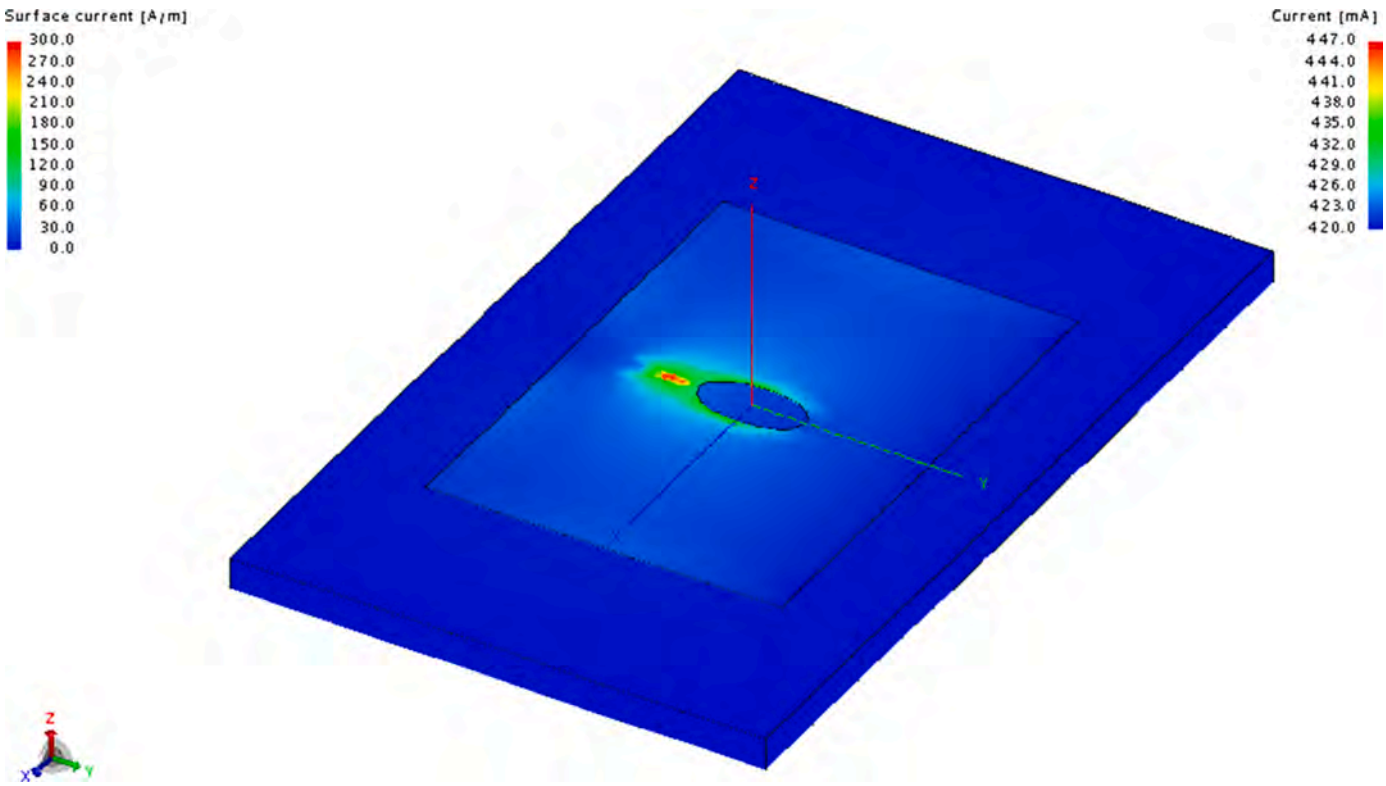

Fig. 5. Current Distribution Magnitude at 2.6 GHz.

slotted patch antenna system design, including the system design parameters, and its various configurations. Section III shows the simulation and experimental results as well as detailed discussion on the fabricated models. The paper is concluded in section IV.

2. Elliptically-slotted patch antenna design

The foundational designs of patch antennas were primarily rectangular or circular microstrip patch antennas. These structures offered a

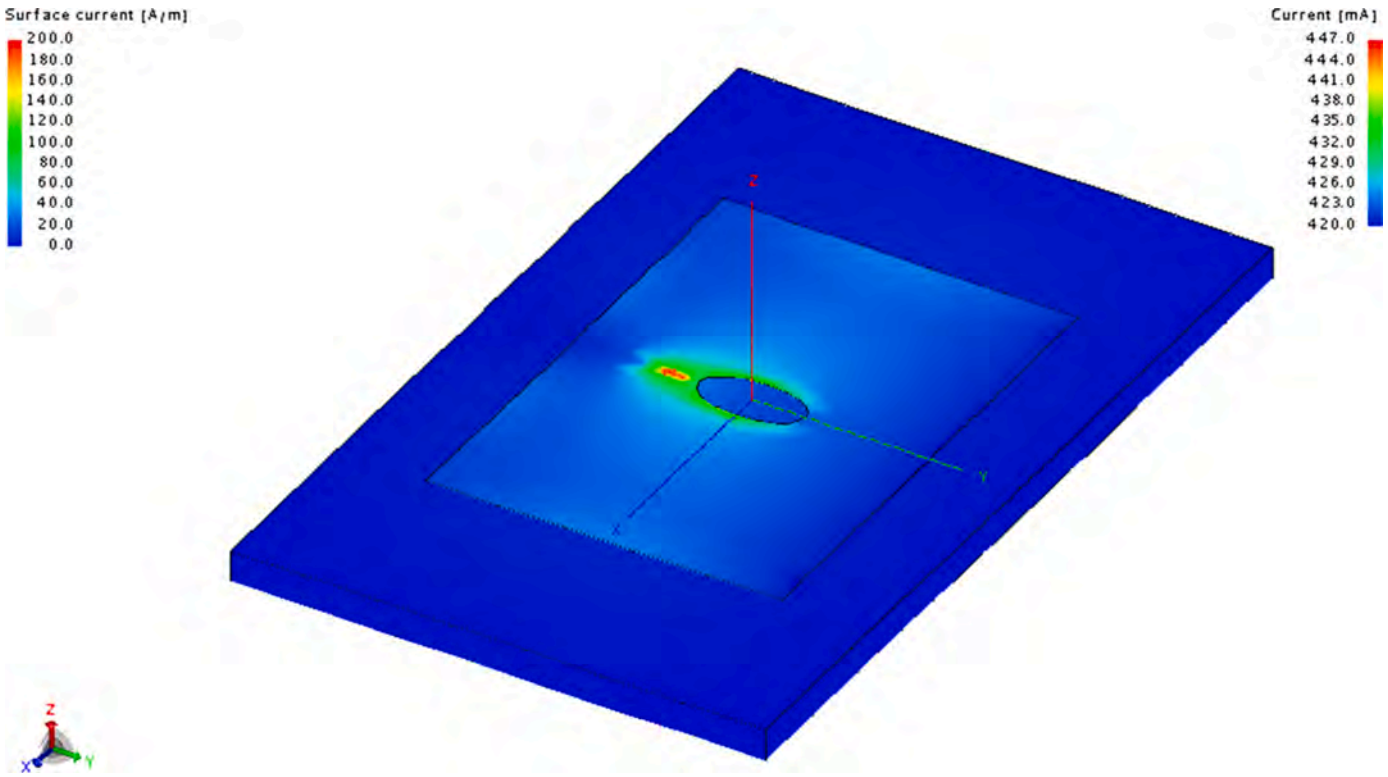

Fig. 6. Current Distribution Magnitude at 2.8 GHz.

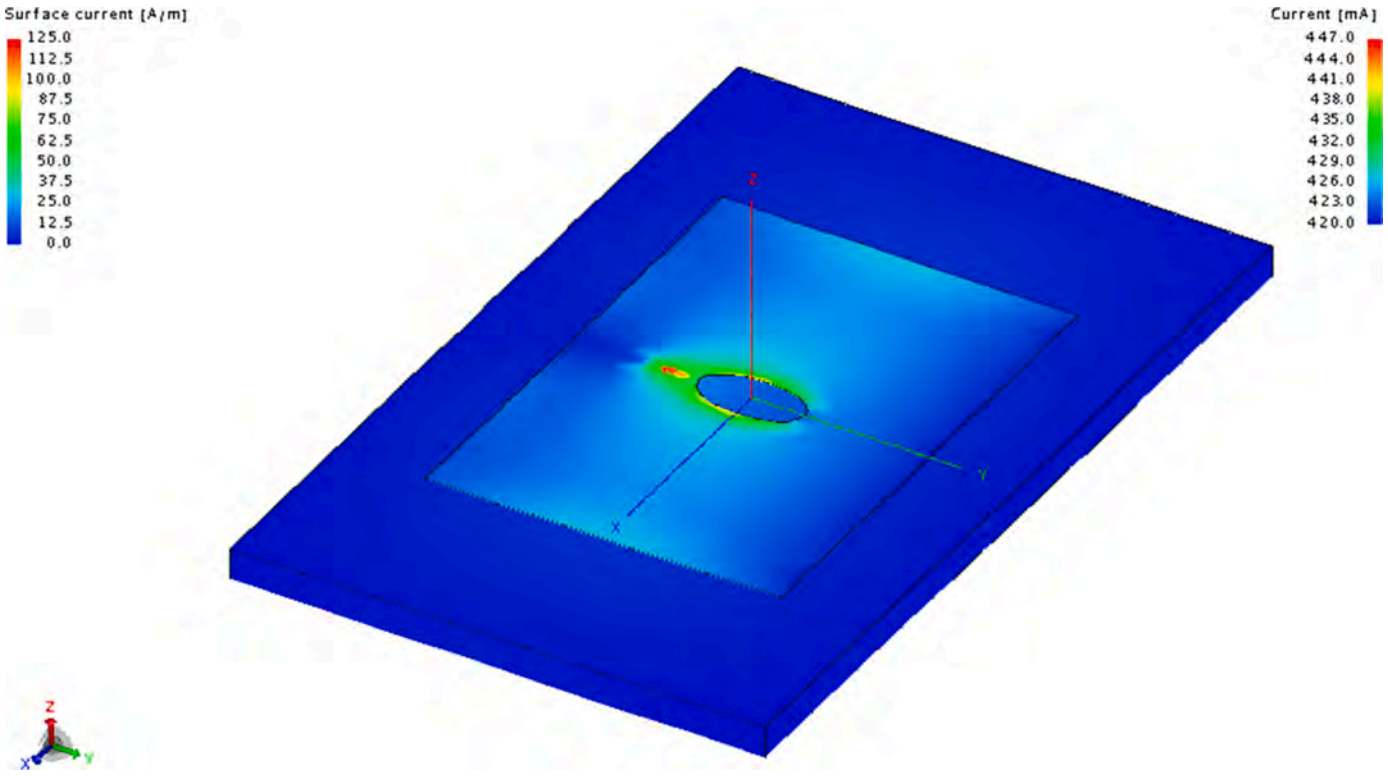

Fig. 7. Current Distribution Magnitude at 3.0 GHz.

basic level of efficiency, simplicity in design, and compatibility with integrated circuits. However, they were typically narrow-banded and required a larger surface area.

To address the inherent limitations of traditional patch designs, researchers began to investigate slot-based modifications. Initial slot designs were straight cuts or circles, which provided slight improvements in bandwidth. The elliptical slot was introduced as an innovative approach to further enhance the patch antenna's bandwidth and multi-

band capabilities. The elliptical shape's inherent geometric properties allowed for enhanced electric field distributions, enabling the antenna to resonate at multiple frequencies.

The primary advantage of using an elliptical slot over a regular patch was the possibility of multi-resonant frequencies [2]. This made the design particularly appealing for applications that required dual-band or multi-band operations. Additionally, the elliptical slot provided an enhanced impedance bandwidth, making it more versatile for various communication applications. The novelty of the elliptically slotted patch antenna is in its good correlation between simulated and real-life models and the very low resonance frequency difference (2.5%) between the finite and the infinite grounds approximations compared with the conventional patch antenna (6.6%). The ESPA model improves both the finite and infinite substrates, thereby eliminating the need for the geometrical size of the finite substrate to be increased to achieve the infinite approximation.

This novel ESPA configuration enables reliable, small footprint and portable antenna systems for multipurpose real-time label-free biosensing and Wi-Fi 6E applications to be developed [21]. With its reduced resonance frequency difference, the novel ESPA fractal is suitable for embedded circuit-emulating non-invasive and non-ionising radiation sensing implementations. Moreover, the directivity of the ESPA configuration changes with the different dielectric substances that interfere with its field distribution. This is a more appealing alternative for specific conventional wireless biosensing transducers and very promising for biosamples identification, selectivity, and profiling. The design technique adopted for the ESPA subsystem development is amendable to digitally assisted multiband, multi-standards reliable, small footprint/form factor and portable RF antenna for Wi-Fi 6E and cellular narrowband IoTs applications [8,22].

2.1. Patch antenna configuration modelling

A model geometry of the proposed novel elliptically-slotted patch antenna (ESPA) system is shown in Fig. 1. The elliptical slot is designed at the centre of the patch to detect the variations in the performance of the antenna with the introduction of a biological sample in it.

The substrate is a Rogers RT duroid® glass fiber reinforced polytetrafluoroethylene (PTFE) composite designed for microstrip circuit applications. The actual patch component is a substrate-centralised elliptically-slotted copper metal with a thickness of 1-1.6 mm. The ESPA system is excited with a pin such as a Subminiature version A (SMA) connector. The ESPA feed assembly is a coaxial cable or probe feed is from underneath through the ground plane as shown in Fig. 2. The outer conductor of the coaxial cable is connected to the finite ground plane and the centre conductor passes through the substrate to the patch antenna. Figs. 3, and 4 present the instantaneous electric and magnetic currents of the ESPA system at 2.8 GHz.

Figs. 5, 6 and 7 depict the magnitude of the current distributions of the ESPA system at 2.6 GHz, 2.8 GHz and 3.0 GHz respectively.

The models of various geometrical shapes are created at the centre of the patch to find the appropriate design for biosample sensing by comparing their performance. The CAD model of the rectangular slotted patch antenna (RSPA) with 5 mm length and 2.5 mm breadth; square-slotted patch antenna (SqSPA) with 5 mm per side; and spherical slotted patch antenna (SpSPA) with 5 mm radius shown in Figs. 8, 9 and 10 respectively.

Mathematically, the resonant frequency, f_r of an RF/Microwave rectangular patch antenna is given by:

$$f_r = \frac{1}{2\pi\left(\sqrt{LC}\right)} \tag{1}$$

where the inductance L initialised into the design through the pin feed and C is capacitance which is directly proportional to the effective permittivity and effective area whereas which is inversely proportional

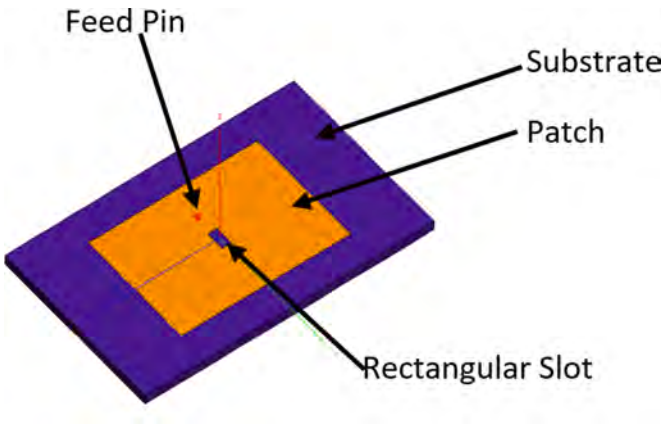

Fig. 8. Rectangularly-Slotted Patch Antenna (RSPA).

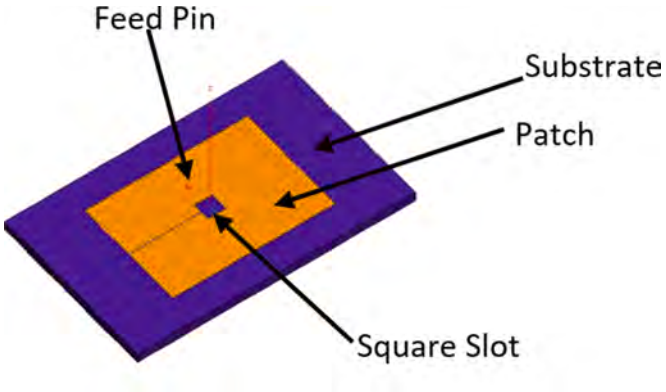

Fig. 9. Squarely-Slotted Patch Antenna (SqSPA).

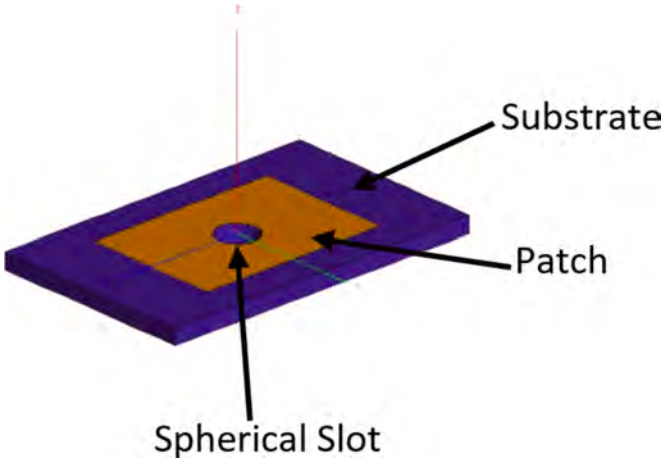

Fig. 10. Spherically Slotted Patch Antenna (SpSPA).

to the thickness of the dielectric substrate. RF range extends from 20 KHz to 300 GHz and commonly used for radio communication purposes.

The parameters which influence the properties of a microstrip patch antenna include the length (l) and width (W) of the patch, height of the substrate (h); and dielectric constant of the substrate (ϵ_r). The operating (centre-design) frequency, f_c, is regulated by the length of the patch and given by:

$$f_c = \frac{c}{2l/\left(\sqrt{\epsilon_r}\right)} \tag{2}$$

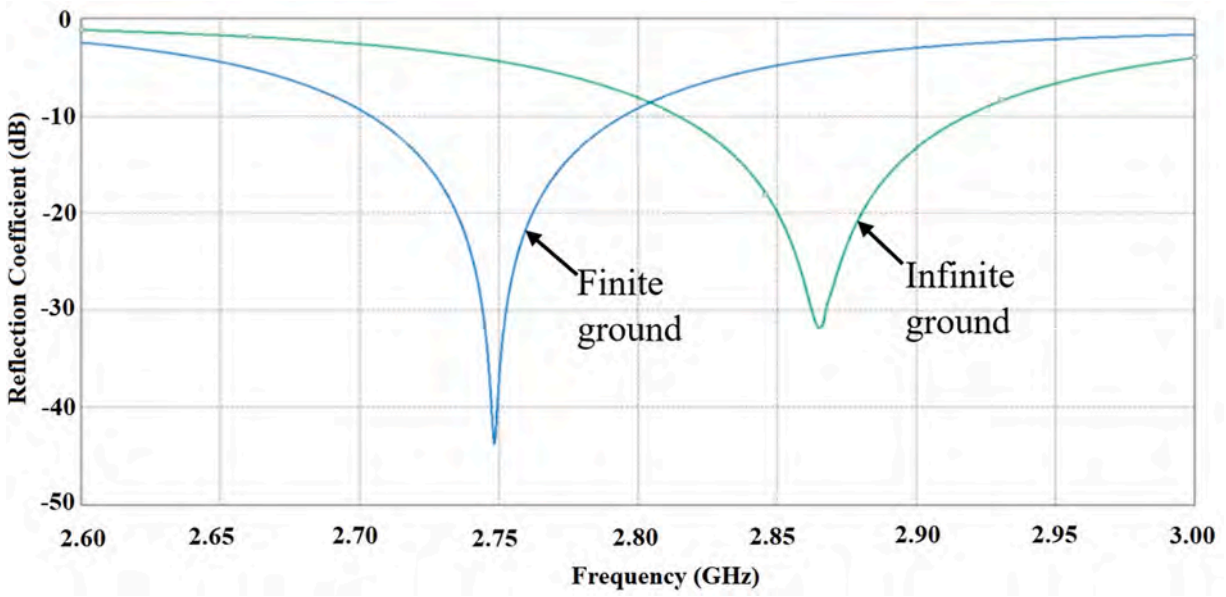

Fig. 11. Reflection Coefficient vs Frequency of RSPA.

Table 1
Performance analysis of RSPA .

Performance Parameter	RSPA values on Finite Ground
Frequency at 50 Ω impedance	2.74 GHz
Gain	6.75 dB

where c is the speed of light in the vacuum (ms^{-1}), (ϵ_r), the relative permittivity of the substrate.

The width of the patch, (W), is derived using:

$$W = \frac{c}{2f_r/\left(\sqrt{(\epsilon_r+1)/2}\right)} \tag{3}$$

The dielectric constant or permittivity of the substrate is a significant parameter that modulates the fringing fields of the antenna and subsequently affects the radiation. The effective dielectric constant, (ϵ_{eff}) takes into account the fringing fields extending beyond the physical dimensions of the patch:

$$\epsilon_{eff} = \frac{\epsilon_r+1}{2} + \frac{\epsilon_r-1}{2}\left(\frac{1}{\sqrt{1+12\frac{h}{W}}}\right) \tag{4}$$

As the permittivity lowers, it leads to broader fringes, which aid to attain preferable radiation. Lower permittivity values have better antenna efficiency and lower impedance values. However, the potential of higher permittivity to reduce the antenna's size is exploited by many fields and gives patch antenna more attention in designing field.

This section's investigational procedure validates the elliptically slotted patch antenna model's quality with other geometrical structures instead of an ellipse. The performance of a rectangular shape at the

Table 2
Performance analysis of SSPA .

Performance Parameter	SSPA values on Finite Ground
Frequency at 50 Ω impedance	2.74 GHz
Gain	6.75 dB

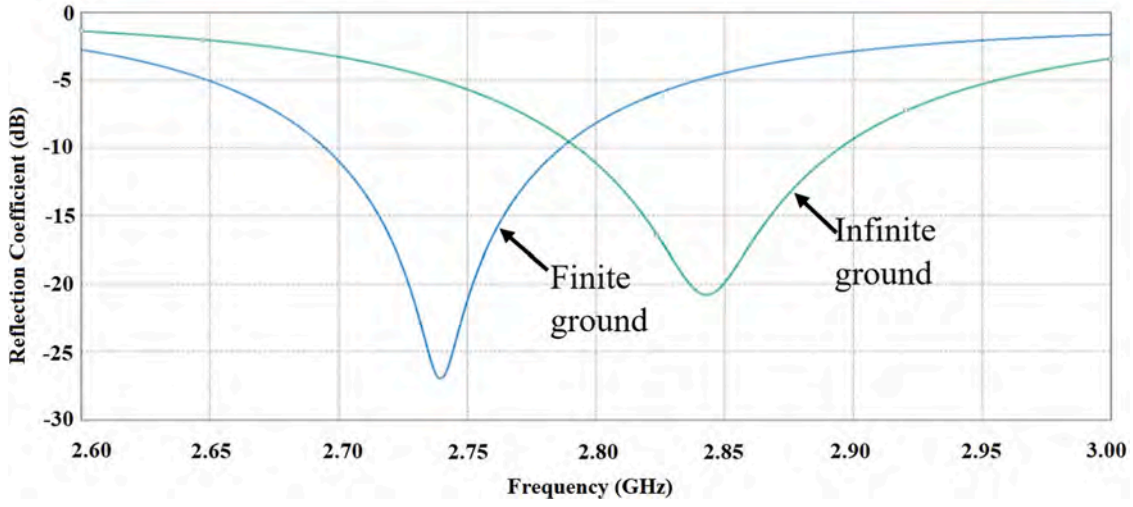

Fig. 12. Reflection Coefficient response of SqSPA.

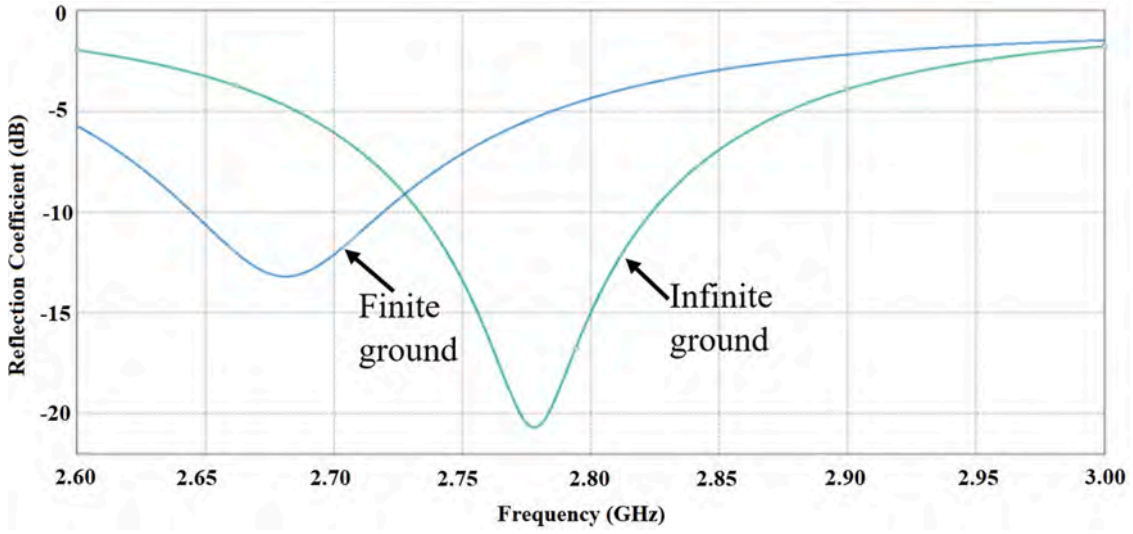

Fig. 13. Reflection Coefficient vs Frequency of SpSPA.

Table 3
Performance analysis of SpSPA .

Performance Parameter	SpSPA values on Finite Ground
Frequency at 50 Ω impedance	2.68 GHz
Gain	6.75 dB

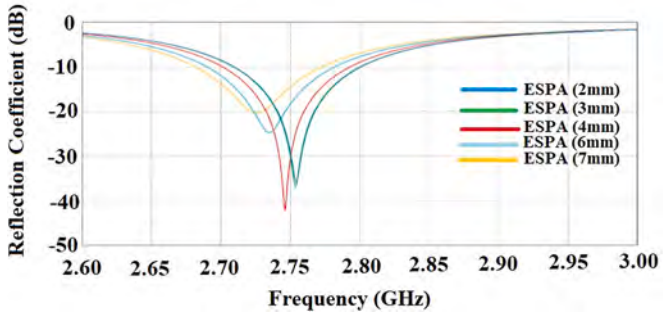

Fig. 14. Differences in ESPA models based on radii on Reflection coefficients.

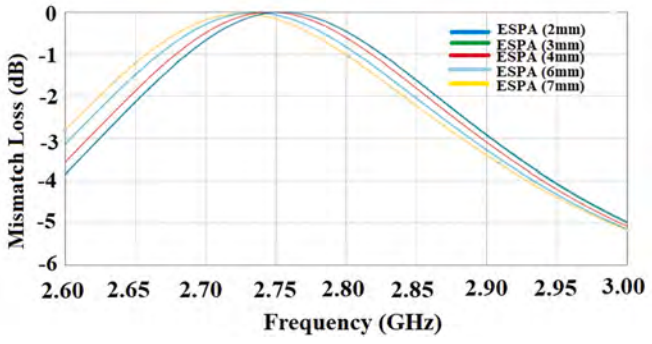

Fig. 15. Differences in ESPA models based on radii on Mismatch loss.

centre of the patch is modelled, and the corresponding reflection coefficient versus frequency graph is shown in Fig. 11.

The rectangular slotted patch antenna (RSPA) resonates at 2.86 GHz on the infinite ground and 2.74 GHz at the finite ground, thereby yielding a 4.1% difference in resonant frequency. Though the centre design frequency is selected as 2.79 GHz, the RSPA system exhibits the same reflection coefficient of approximately -9.1 dB at a frequency of 2.81 GHz. This result depicts a precise performance analysis of RSPA, showing that the ESPA model has preferable behaviour than the RSPA.

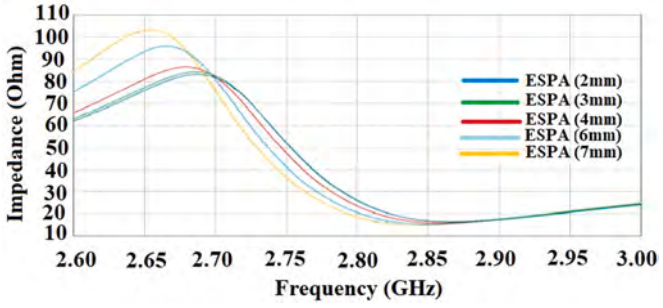

Fig. 16. Differences in ESPA models based on radii on Impedance Magnitude.

The performance responses of the RSPA to the impedance magnitude and total gain are shown in Table 1. The second pattern, which explored for the comparison is a square shape and the centre of patch antenna modelled such a way to generate a square slotted patch antenna (SqSPA). From Fig. 12, the resonating frequencies of the SqSPA model are 2.84 GHz on the infinite ground and 2.74 GHz on the finite ground. The resonance frequency difference for this model is about 3.8%, which is better than RSPA; however, it is not as efficient as the ESPA model. The finite and infinite response of SqSPA system resonates together close to the design frequency at a reflection coefficient value of -9.5 dB.

Table 2 illustrates the performance of SqSPA. From the values, it is clear that the potential of SqSPA displays a better performance compared with RSPA. The third structure, which modelled and analysed in this section, is a spherical model at the centre to place the biosample and its performance in terms of reflection coefficient versus frequency shown in Fig. 13. Unlike other geometrical shapes, the spherical model exhibits a significant frequency shift from the designed frequency and thus not suitable for biosensing applications. However, the patch antenna resonates at 2.77 GHz on the finite ground and 2.68 GHz on the finite ground, resulting in a difference of 3.2% in its resonance frequency. Though it yields an acceptable difference, the same reflection coefficient of -9.1 dB occurs at a frequency of 2.72 GHz.

Table 3 illustrates the performance of SqSPA. From the values, it is clear that the potential of SqSPA displays a better performance compared with RSPA.

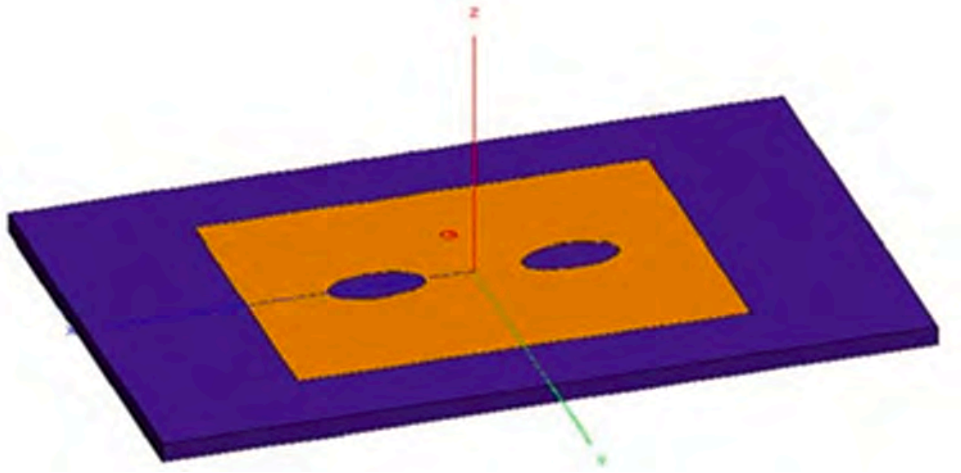

Fig. 17. Second-Order ESPA System Model.

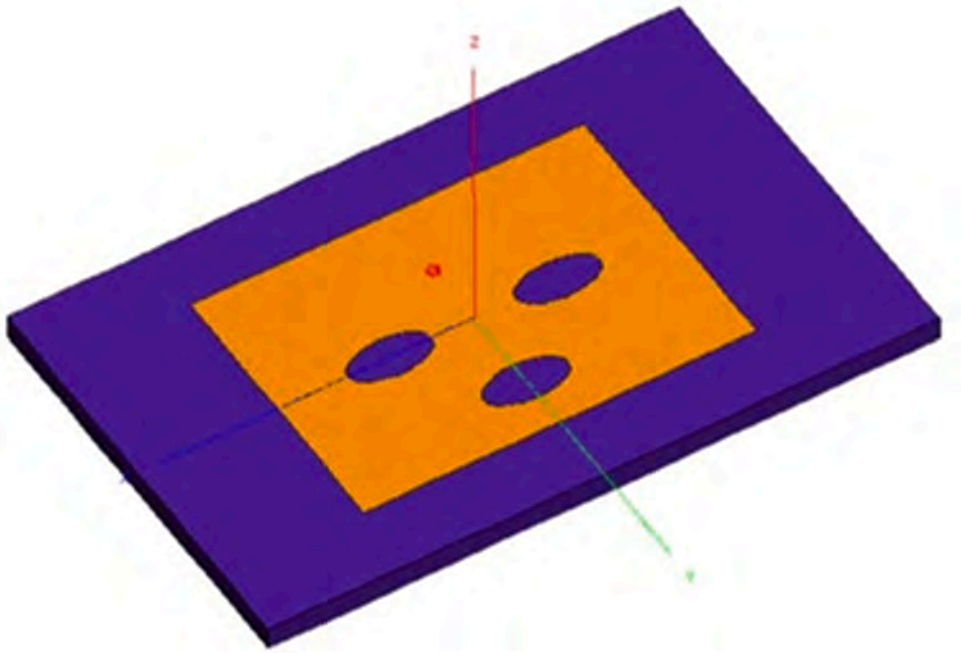

Fig. 18. Third-Order ESPA System Model.

2.2. Performance of ESPA on radii differences

The radii of the ellipse to create the ESPA model selected has a major axis of 5 mm and a minor axis of 2.5 mm. The difference in the reflection coefficients, mismatch loss, and impedance of ESPA is summarized in Figs. 14, 15 and 16 respectively.

From this, it is clear that the basic ESPA model's radius is better compared with other radius choices. The slots' effect in a rectangular microstrip patch antenna is affected by the increment in the slot size and can decrease antenna frequencies. The second-order model is shown in Fig. 17.

Figs. 18 and 19 show the third-order configurations with various positioning of the ellipses. However, the second method of third order ESPA was designed so that three ellipses joined together towards the centre of the patch.

Fig. 20 shows the fourth order ESPA with four ellipses on the patch with a distance of 20 mm and 14 mm between the centres of ellipses horizontally and vertically, respectively.

3. Result and discussion

3.1. Antenna gain and efficiency

The antenna efficiency (or radiation efficiency), ϵ_R can be written as the ratio of the radiated power, $P_{radiated}$, to the input power, P_{input}, of the antenna:

$$\epsilon_R = \frac{P_{radiated}}{P_{input}} \tag{5}$$

Fig. 21 shows the plot of the antenna gain vs frequency. At a design frequency of 2.8 GHz, the gain of the designed antenna is approximately 6.2 dBi.

Fig. 22 shows the axial ratio of the designed antenna. The lower axial ratio value is due to the bespoke geometry design and feeding

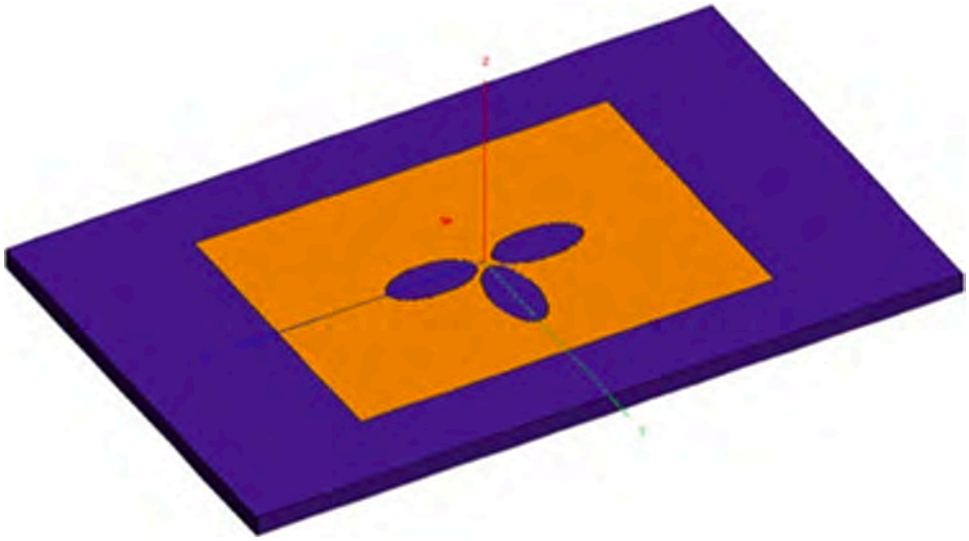

Fig. 19. Third-Order ESPA System Model (Closer Approach).

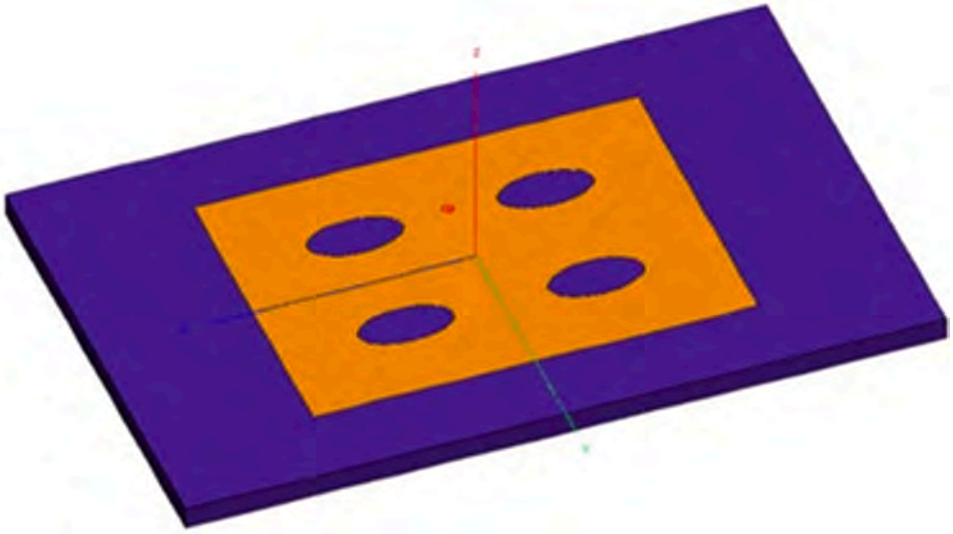

Fig. 20. Fourth-Order ESPA System Mode.

mechanism of our antenna.

The total efficiency, ϵ_T, of an antenna is the radiation efficiency, ϵ_R, multiplied by the impedance mismatch loss of the antenna, M_L, when connected to a transmission line or receiver (radio or transmitter). This can be summarized in equation:

$$\epsilon_T = M_L \times \epsilon_R \tag{6}$$

Considering a centre design frequency of 2.8 GHz, source excitation of 1 V, 0°, 50 Ω, this yields an input power of 0.02 W. The radiated power (Fig. 23) at 2.8 GHz is approximately 15 mW. The mismatch loss at 2.8 GHz (Fig. 24) is 0.95. The radiation efficiency is calculated to be 0.75.

Therefore the total efficiency, ϵ_T, at 2.8 GHz, is given by:$M_L \times \epsilon_R$=0.95× 0.75=0.7125=71%

3.2. Performance of CSPA versus ESPA

The outstanding potential of electronic technologies exerted into the biotic field to understand the physiological variations in the body and ultimately leads to the development of biosensors. The active sensing part that acts as a biosensor in this investigation is the patch antenna, and the performance of conventional slot-less patch antenna (CSPA) is compared with the elliptically slotted patch antenna (ESPA). The model's operating frequency is selected as 2.79 GHz with a frequency range of 2.6 GHz and 3.0 GHz. The design specifications of this first-order ESPA model is in Table 4.

The models of both antenna systems are created, and the performance is analysed on finite and infinite grounds. The infinite system designed such that the ground is a planar multilayer substrate with layer one as a perfect electric conductor (PEC) with a thickness of substrate height whereas, a homogeneous, free space medium is considered for finite ground design. Figs. 25 and 26 give the reflection coefficient response for CSPA and ESPA systems respectively.

The resonating frequencies of CSPA on the infinite ground are about 2.87 GHz and 2.70 GHz on the finite ground. This conventional patch antenna system introduces a general difference of 5.9% in its resonance frequency. However, the designed ESPA model resonates at 2.83 GHz on the infinite ground and at 2.74 GHz on the finite ground with a resonance frequency difference of about 3.1%. A considerable improvement of almost 2.8% of the CSPA model is achieved using the proposed design. Any sensor design based on electromagnetic principles should exhibit an

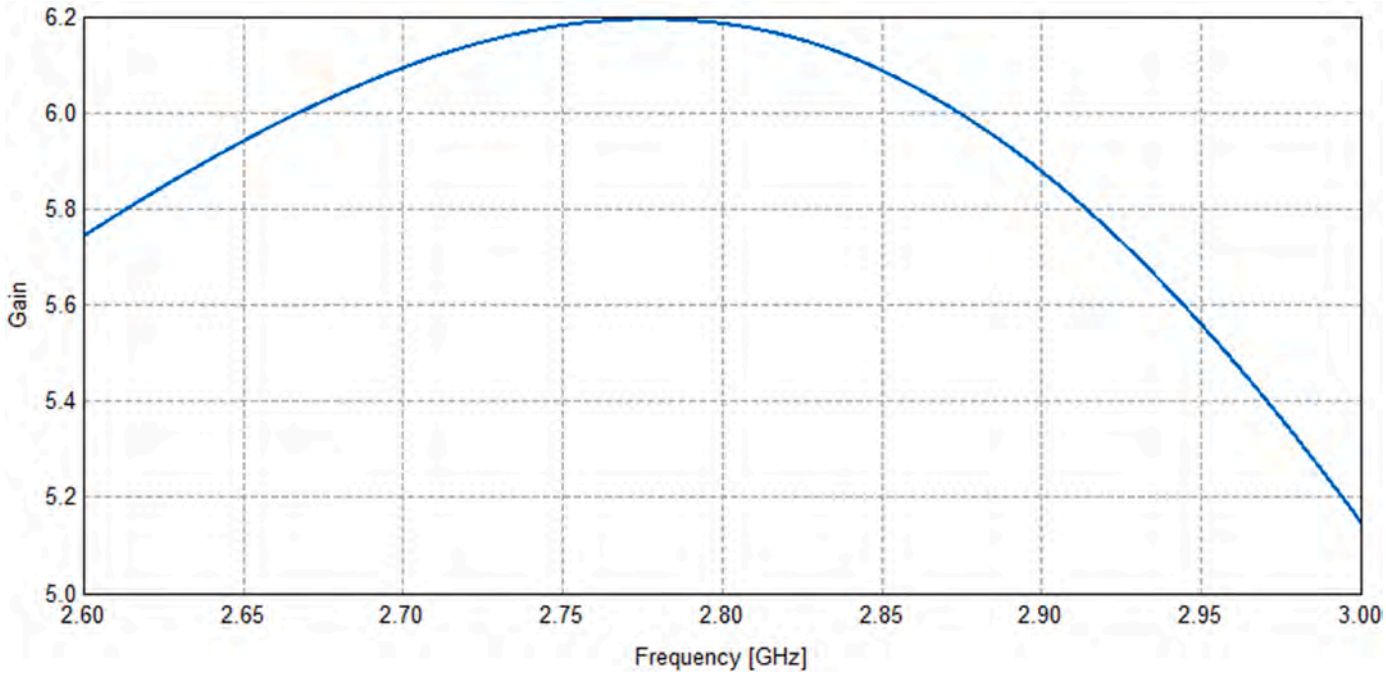

Fig. 21. Antenna Gain vs Frequency.

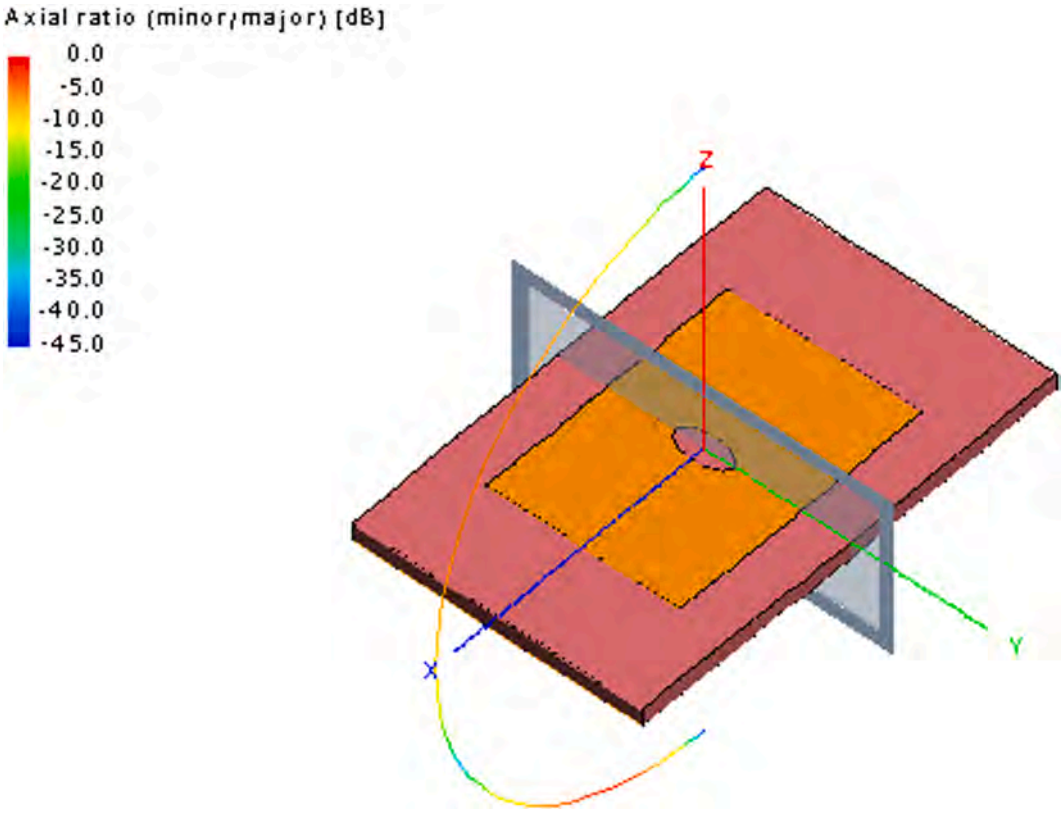

Fig. 22. Axial Ratio of designed antenna.

acceptable interrelationship with simulated and real-life models. The concurrence of reflection coefficient values on infinite and finite grounds of CSPA is approximately -6.0 dB (Fig. 25) whereas, it is much better in ESPA with -11.0 dB (Fig. 26) at the operating frequencies.

The geometrical size of the ESPA system modulated such that it emulates with the infinite estimation as the practical implementation follows the simulated designs. The system is flexible in terms of its weight and portability and even allows the merging of designs based on meta-materials, improving the bio-sensing capabilities. The impedance magnitude of the ESPA system is shown in Fig. 27. In any given RF design, there is a factor that opposes the designed system known as impedance and the proposed ESPA model achieved a characteristic

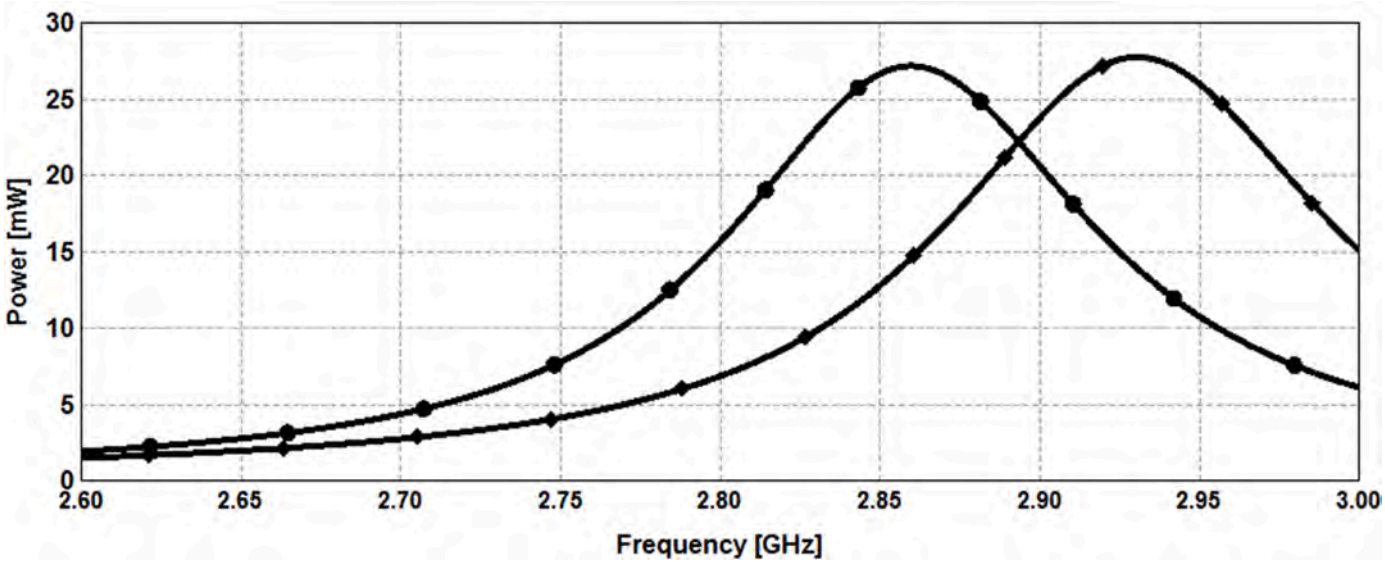

Fig. 23. Radiated Power vs Frequency plot.

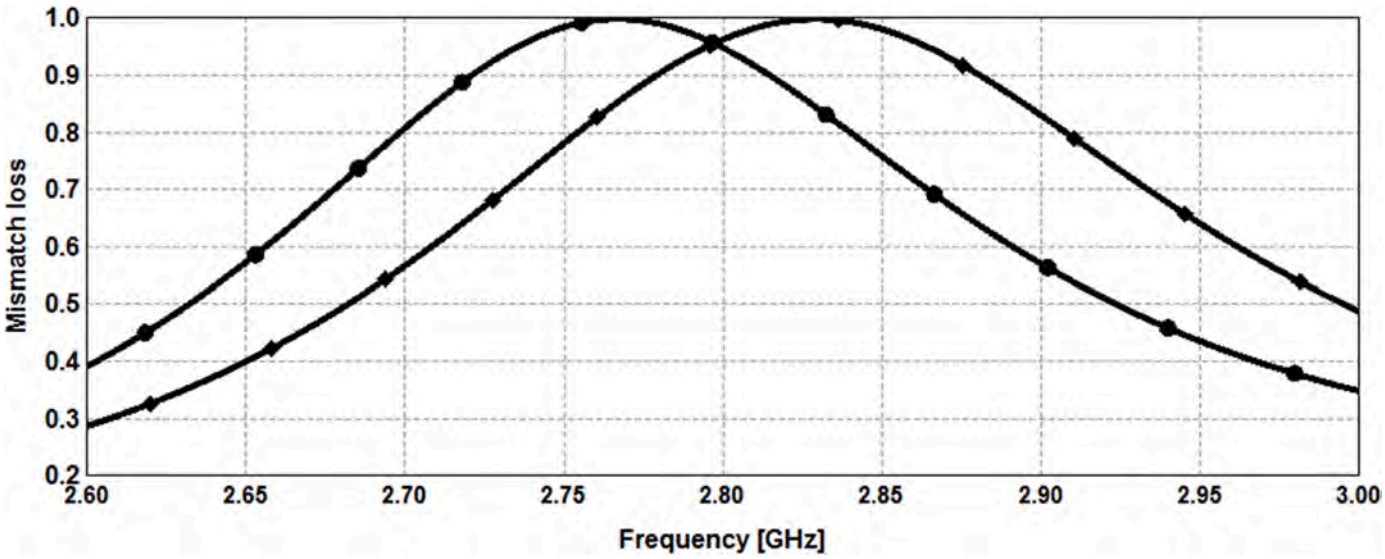

Fig. 24. Mismatch loss vs Frequency plot.

Table 4
Design specifications of the first order ESPA model .

Model Parameter	Value (mm)
Patch Width	46.8
Patch Depth	33.2
Substrate Height	2.87
Substrate Width	80
Substrate Depth	50
Feed Distance	8.9
Feed Radius	0.65
Minor Radius of Ellipse	2.5
Major Radius of Ellipse	5

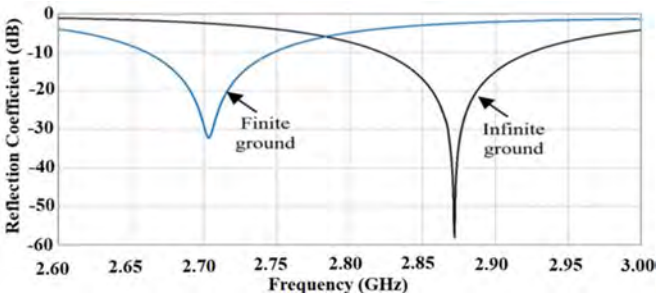

Fig. 25. Reflection Coefficient response (CSPA).

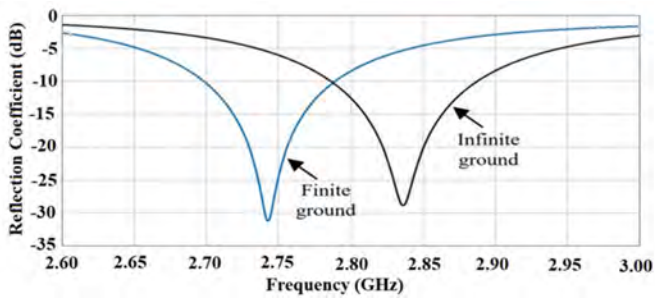

Fig. 26. Reflection Coefficient response (ESPA).

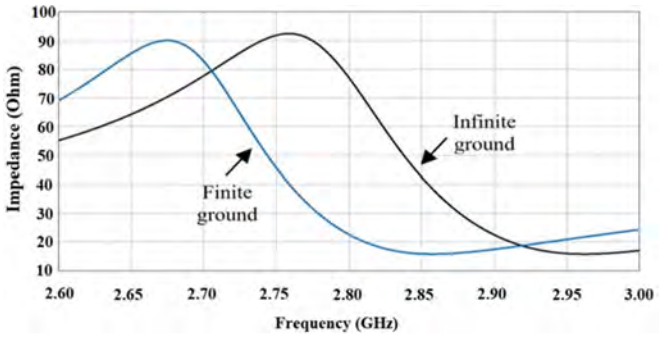

Fig. 27. Impedance Magnitude of the ESPA System.

impedance of 50 Ω at a frequency of 2.74 GHz.

To improve the power transmission from source to load, an impedance matching circuit is a crucial criterion in biosensors development. Such a design leads to a balanced system with less interfered signals in bio-sensing applications. Fig. 28 depicts the ESPA system's radiation pattern with a total gain of 6.75 dB in the vertical orientation.

Fig. 29 give the reflection coefficient versus frequency for the second-order ESPA configuration. The second-order model resonates at about 2.66 GHz on the finite ground and 2.74 GHz on the infinite ground with a resonance difference of about 2.9%. Second-order model exhibits a 0.2% drop in its difference from the first-order ESPA with a frequency shift of almost 0.1 GHz. The simulated model with two ellipses generates the same reflection coefficient of -9.8 dB at 2.69 GHz.

The characteristic impedance of 50 Ω appears at the resonating frequency of 2.66 GHz on the infinite ground and is shown in Fig. 30. It is evident that the correlation of impedances on the finite and infinite ground occurred at 2.62 GHz with the same impedance magnitude of 89.8 Ω. The second-order system's radiation pattern is linearly polarised with a total gain of 6.0 dB at 2.8 GHz.

Fig. 31 shows the frequency response to the reflection coefficient of the third-order configuration. This model's resonating frequency shifted away from the designing frequency to about 2.64 GHz with a reflection coefficient value of 15.05 dB on the finite ground. The third-order resonating frequency on the infinite ground is almost 2.72 GHz with a reflection coefficient value of -14.5 dB. The resonance frequency difference is further reduced by about 0.4% from the second-order configuration and which is approximately 2.5% in the third-order configuration. The models give the same reflection coefficient of about -9.8 dB at 2.68 GHz. Both second and third-order models show similar reflection coefficient values at the matched models with an approximate difference of about 2 dB from the basic ESPA model.

The impedance magnitude with characteristic value is exhibiting on its resonant frequency with a 0.09 GHz from the first-order model and

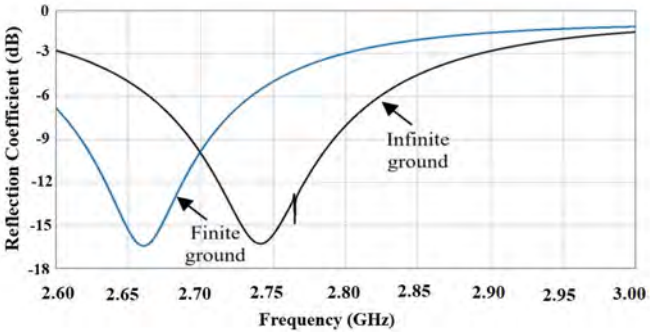

Fig. 29. Reflection coefficient response for the second-order ESPA configuration.

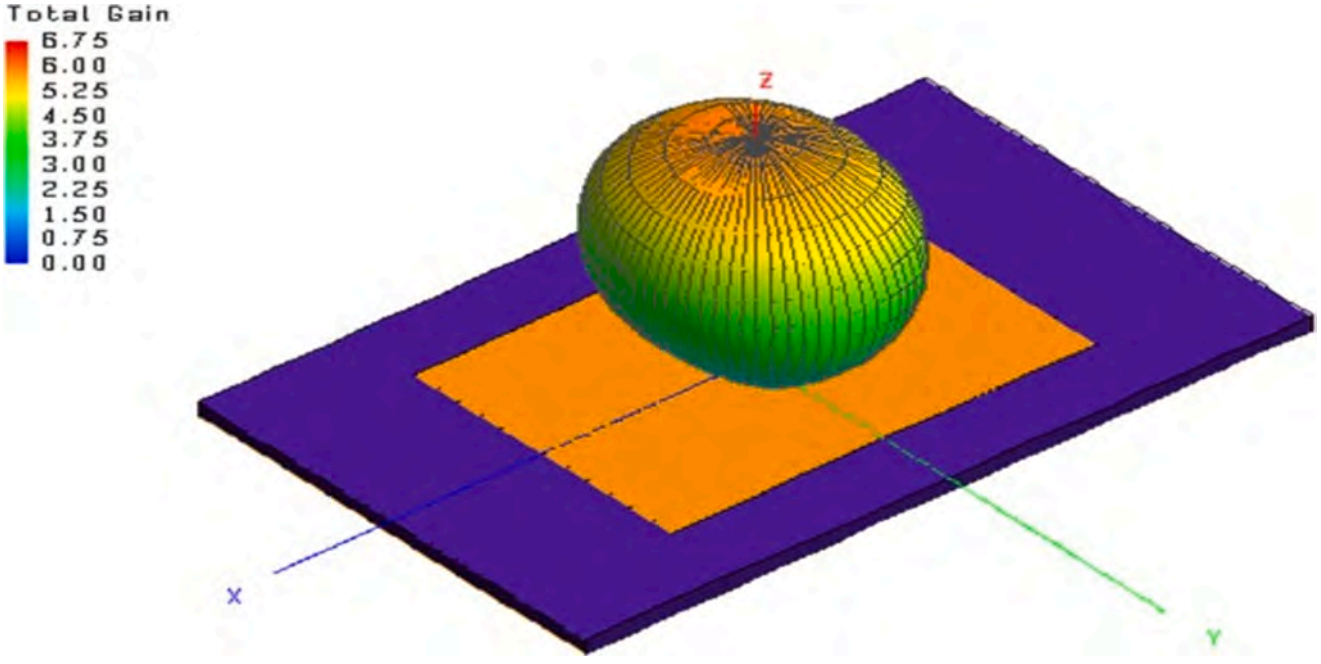

Fig. 28. Radiation Pattern of the ESPA System at 2.8 GHz.

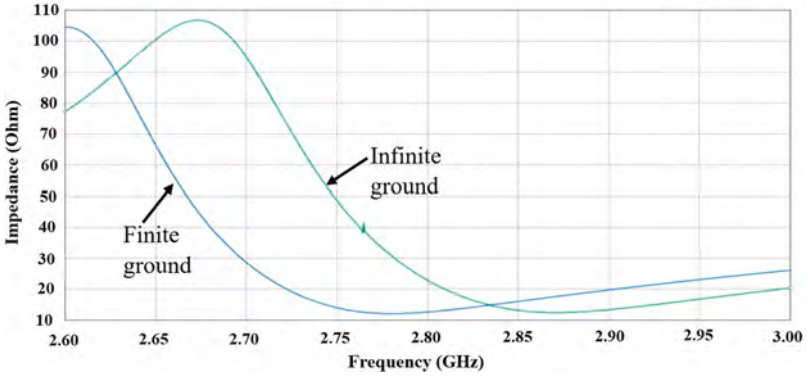

Fig. 30. Impedance magnitude plot vs frequency.

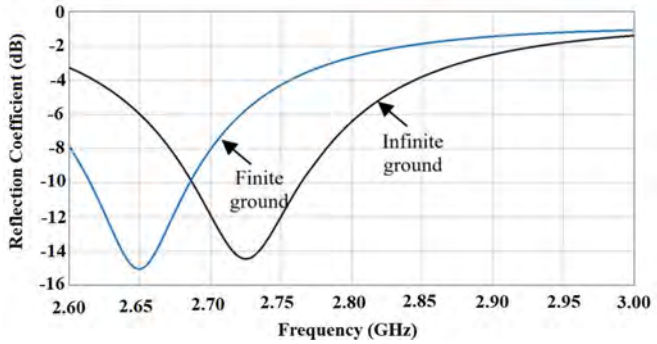

Fig. 31. Frequency response in relation to the reflection coefficient of the third-order configuration.

shown in Fig. 32.

The radiation pattern shows a similar gain as that of the second-order ESPA system. Fig. 33 represents the frequency response of another third-order model with variations in the alignment of the ellipses. The system shows same resonance difference in both models with three ellipses irrespective of the location. However, there is a significant change in its reflection coefficient values compared with the prior model. The finite model resonates with a reflection coefficient value of 12.4 dB, whereas it is about -11.7dB for the infinite model with the same value at -9.35 dB.

The third-order model resonates at 2.66 GHz, which is about 0.13 GHz away from the designed frequency (Fig. 34). This frequency shift attributed to the presence of more ellipses at the rectangular patch.

Fig. 35 shows the reflection coefficient versus frequency of the fourth-order configuration. The model with four ellipses on the finite ground resonates at 2.65 GHz and on the infinite ground resonates at 2.71 GHz. The resonance frequency difference is reduced to 2.2%, which is about a 0.9% drop from the first-order model.

The first-order ESPA was designed to work on 2.79 GHz, but it is resonant at 2.74 GHz. It is evident from the further order configurations that the resonant frequency shifts away from the design frequency. As the number of ellipses increases, the fringing fields around the antenna contributes to the frequency shift. Fig. 36 shows the fabricated ESPA fractals.

3.3. *Experimental procedures and proceedings*

This section introduces the designed patch antenna's experimental and test procedures (Fig. 37). The major requirement for the model's testing is the spectrum analyser, and used in this project is N9917A 18 GHz FieldFox Microwave Analyzer, provided by Keysight Technologies. The patch antenna connected to the analyser through N9910X-701 Rugged phase-stable cable of Type N (m) to Type N (m) and the coaxial adapter provided within the analyser kit. The S_{11} parameter values of the fabricated patch antenna are available on the spectrum analyser and shown is in Fig. 38. From Fig. 38, the presence of reflections from the antenna is visible. The variations in the expected results from the simulation indicate certain reflections from the patch antenna. This is mitigated by designing an impedance matching circuit at the antenna with the assistance of Advanced Design System (ADS) software provided by Keysight Technologies. The block diagram of impedance matching concept with the antenna is given in Fig. 39. The source used for the antenna is usually a standard source of either 50 Ω or 75 Ω, and the design based on the operating frequency of 2.79 GHz. To make a new schematic of the matching network design, the input impedance to the antenna at the working frequency is required. Table 5 shows the frequency vs S_{11} values obtained from ADS.

A graphical representation of the reflection coefficient values with respect to the frequencies from 1 dB to 5 dB are shown in Fig. 40. The value of S_{11} parameter before matching shows -1.629 dB at 2.79 GHz.

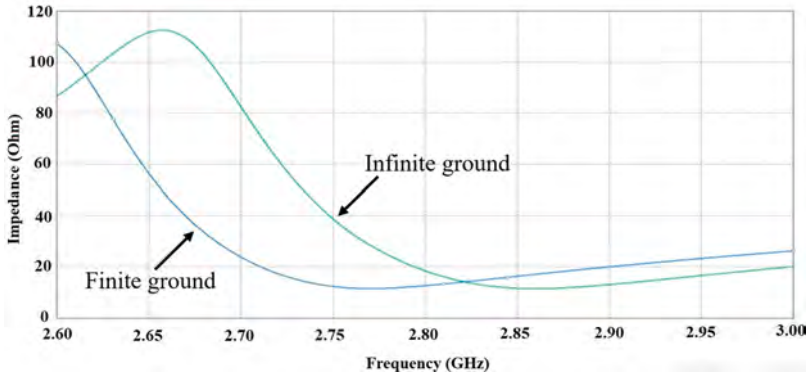

Fig. 32. Impedance magnitude with characteristic value.

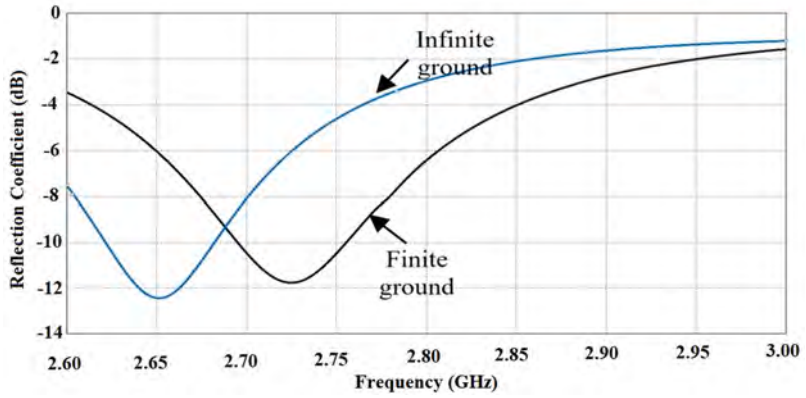

Fig. 33. Reflection Coefficient response of Third- Order ESPA (Closer Approach).

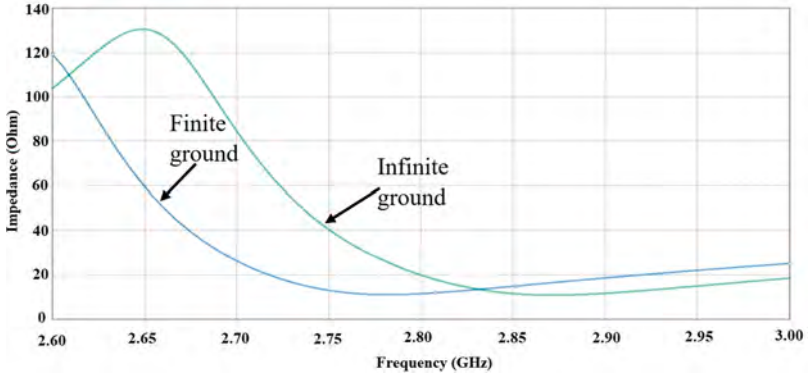

Fig. 34. Impedance response of the Third- Order ESPA (Closer Approach).

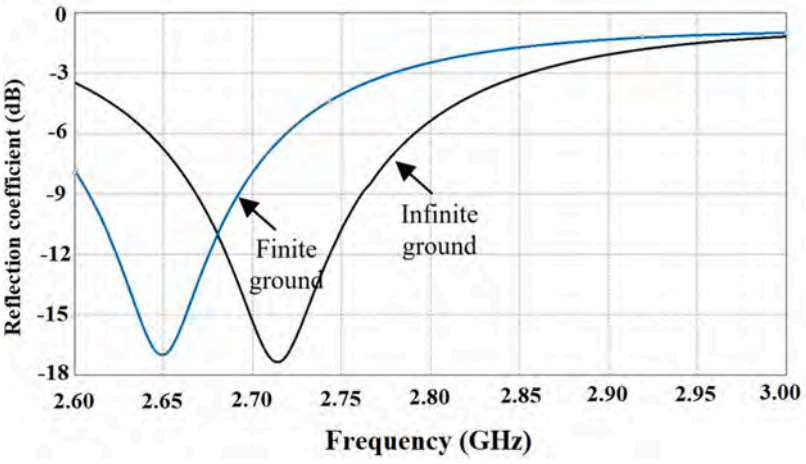

Fig. 35. Reflection Coefficient response of the Fourth-Order ESPA.

The S_{11} values of the antenna measured from the spectrum analyser, is used for matching. The conjugate of the impedance at operating frequency is added to the desired location within the smith chart section and thereby selecting an appropriate network from the options provided by ADS. A low pass LC network is selected so that it passes only the desired frequency and neglects all other higher frequencies that reflects from the load. An inductance of value 5.23 nH and a capacitor of value 1.761828 pF is designed with the assistance of ADS software and simulated the S_{11} response for antenna and obtained as in Fig. 41.

Fig. 42 shows the S_{11} response after matching. There is an enormous improvement of -14 dB at a frequency of 2.6 GHz after impedance matching.

3.4. Performance of ESPA with complex dielectric properties of biosamples

The dielectric properties of biosamples can be introduced into the ESPA model by creating a cylindrical shape at the centre of the ellipse. The properties such as density, relative permittivity, loss tangent and conductivity are initiated into the cylinder at the ellipse centre to behave like a bio- sample for the simulation.

Fig. 43 indicates the frequency response comparison of the first-order

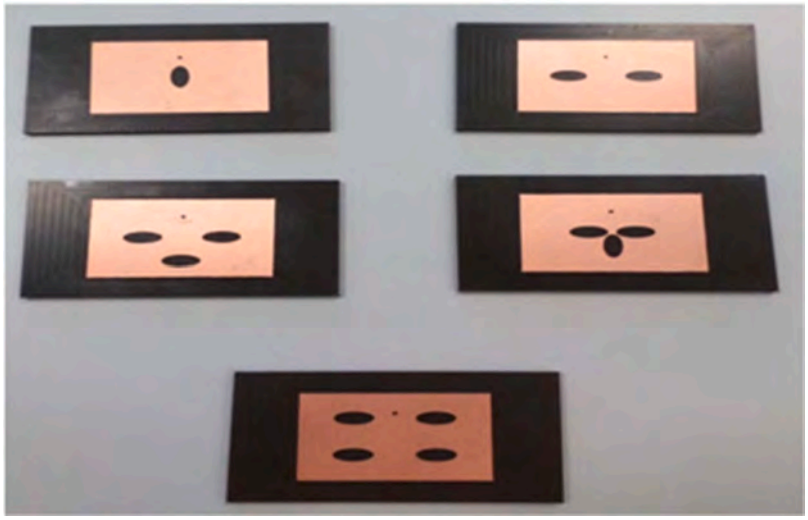

Fig. 36. Fabricated ESPA models.

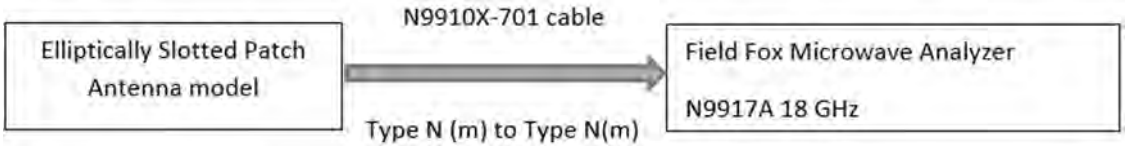

Fig. 37. Measurement setup for the ESPA.

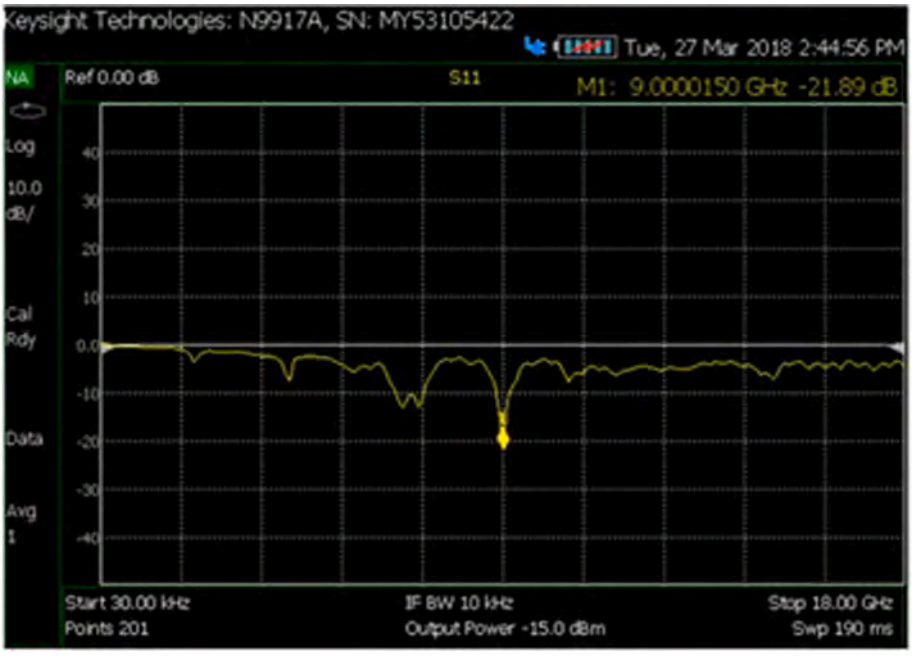

Fig. 38. Measured S_{11} response of the ESPA.

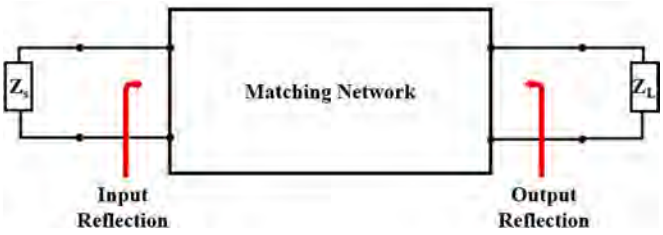

Fig. 39. Impedance matching concept.

Table 5
Design specifications of the first order ESPA model .

Frequency (GHz)	S_{11} (dB)
2.0	-2.246
2.1	-2.858
2.2	-2.033
2.3	-1.394
2.4	-1.224
2.5	-1.271
2.6	-1.442
2.7	-1.768
2.8	-1.733
2.9	-1.629
3.0	-1.563

ESPA on the finite ground and the ESPA with the properties of blood. The finite ESPA with a single ellipse resonates at 2.74 GHz, and the model with blood properties resonates at 2.75 GHz with about -31.5 dB.

Fig. 44 shows the reflection coefficient versus frequency for the basic ESPA system and the system with the dielectric properties of fat at the centre of the ellipse. The ESPA with fat resonates at about 2.74 GHz which is similar to the previous one but, with a significant variation in its reflection coefficient value of approximately -30 dB. The variation in the values of reflection coefficients are critical as this is responsible for detecting the changes in each bio-sample.

Unlike contrasting with the ESPA on the finite ground, the frequency response of two bio-samples such as blood and cortical bone with their dielectric properties are shown in Fig. 45.

The choice of microstrip patch antenna for the biosensor design helped the proposed design to provide a miniaturised size for the system. A thick dielectric material with a smaller value of the dielectric constant can produce better radiation efficiency. However, the minimum size, weight and power-to-cost (SWaP-C) requirements present challenging design considerations. The lower the SWaP-C design solutions, the more the conceptual design and the mission objectives align together. Hence, the presented ESPA antenna finds extensive multipurpose communication and biosensing applications in co-operative satellite-cellular convergence ecosystem networks, Integrated sub-6 GHz 5G/Wi-Fi communication systems need multipurpose transceiver frontend antennas to operate with the SWaP-C design objectives.

The fabrication cost of patch antennas is comparatively lesser than other traditional antenna models and enables mass manufacturing. The lightweight and robust nature of the microstrip patch antenna enhances the system's possibility to be used in real life. However, spurious radiations because of the patch, slots, feed points, and any other connection points may affect the overall efficiency of the system. Moreover, the dielectric and conductor losses, along with cross polarisation radiation, affects the system negatively. Another major area of concern is the lower power managing capacity and intrinsic lesser impedance bandwidth. The introduced system holds several advantages over disadvantages.

Table 6 shows a comparison of the designed patch antenna with other states of the art antennas within the sub-6 GHz frequencies.

4. Conclusion

This paper presents the design of an RF multi-band elliptically slotted patch antenna for cancer detection and bio-sensing applications. The proposed system consists of various order configurations with the insertion of more fractals, exhibiting a significant improvement in its resonance differences on finite and infinite grounds. The sensitivity of the system is tested using the dielectric properties of bio-samples within the ellipse. The variations in the reflection coefficient corresponding to each sample promises the viability of the system in bio-sensing applications. The resonance frequency difference is reduced to 2.2%, which is about a 0.9% drop from the first-order model. The ESPA model is more fitting for real-time bio-sensing applications as the scaled down chip size leads to easy fabrication with low cost. The designed ESPA model

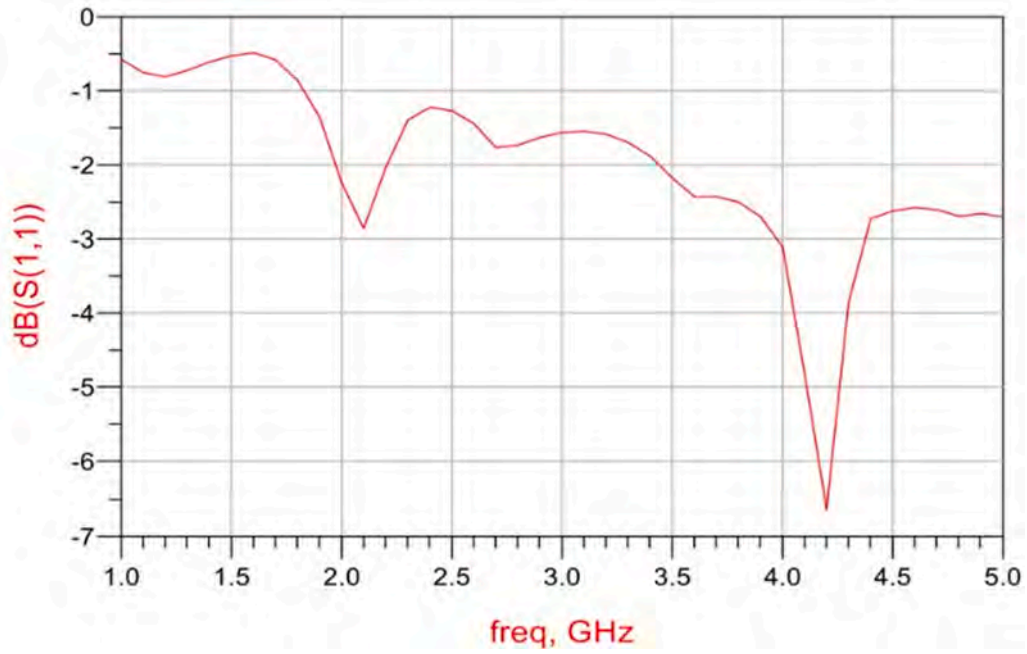

Fig. 40. Frequency response before matching.

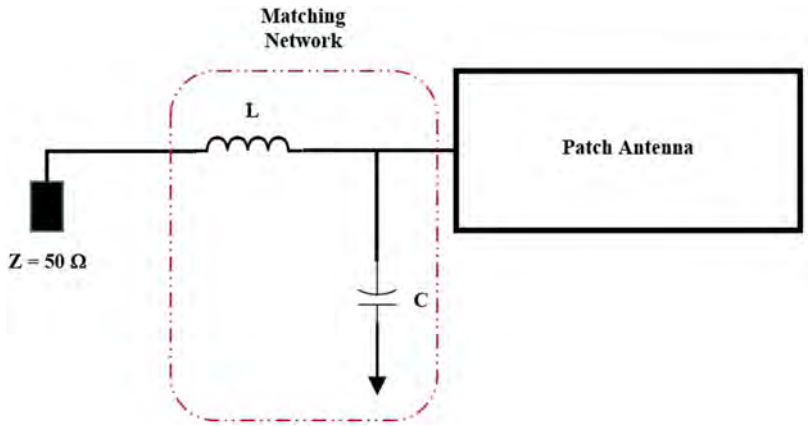

Fig. 41. Matching network for designed patched antenna.

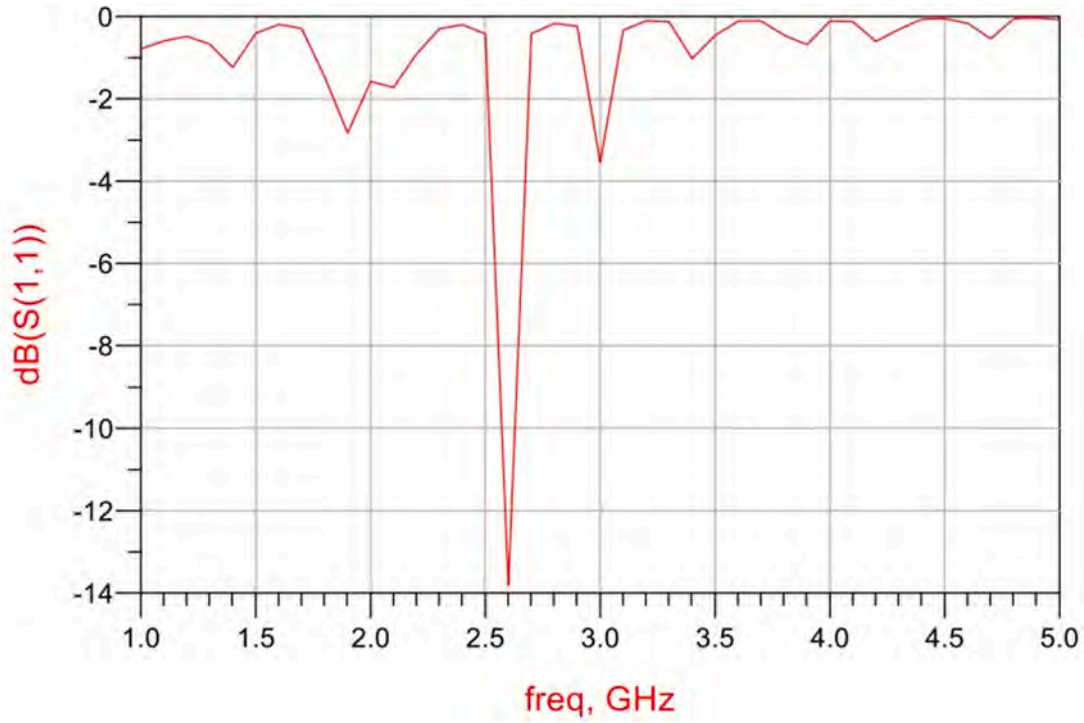

Fig. 42. Matched patch antenna's S_{11} response at 2.790 GHz design frequency.

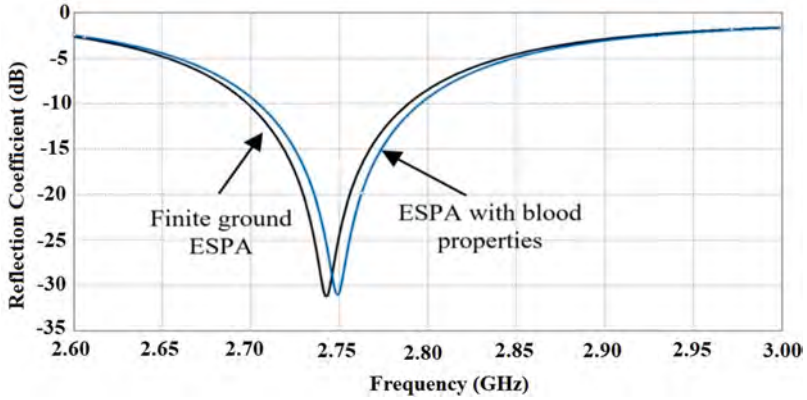

Fig. 43. Reflection Coefficient response of ESPA (with properties of blood).

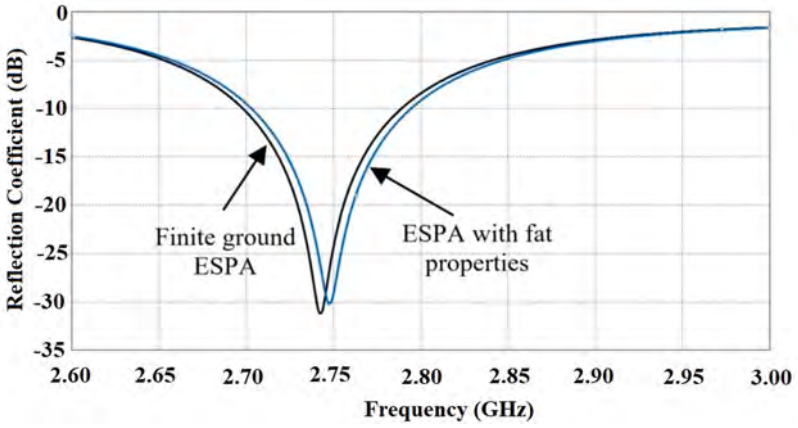

Fig. 44. Reflection Coefficient response of ESPA (with properties of blood and cortical bone).

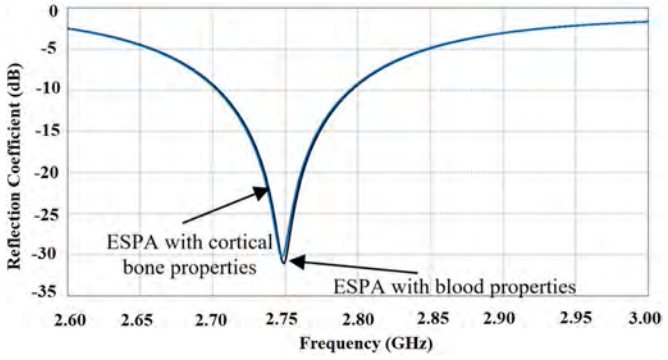

Fig. 45. Reflection Coefficient response of ESPA (with properties of blood and cortical bone).

Table 6
Comparison of designed antenna with other state-of-the-art antennas for 2.4 GHz ISM band and sub-6 GHz wireless applications.

Reference	Antenna Type	Designed Frequency	Gain (dB)
[23]	Tunable	2.6	3.3
[24]	Dual-polarised	2.40-2.65	7.85
[25]	Microstrip	2.5-2.7	6–7
[26]	Microstrip	3.5	2.3
[27]	Microstrip	3.5	7.07
[28]	Microstrip	2.4	1.3
[29]	Microstrip	3.5-5.5	6.86
[30]	Microstrip stub	2.42-7.45	1.5
This Work (2nd-order)	Elliptically-slotted	2.74	6
This Work (3rd-order)	Elliptically-slotted	2.64	6
This Work (4th-order)	Elliptically-slotted	2.65	6

promises to be a vital integration within a reconfigurable transceiver architecture, to investigate the effect of biosamples in the sub-6 GHz 5G frequencies.

Declaration of Competing Interest

The authors declare that they have no known competing financial interests or personal relationships that could have appeared to influence the work reported in this paper.

Data availability

No data was used for the research described in the article.

References

[1] M. Wen, Q. Li, K.J. Kim, D. López-Pérez, O.A. Dobre, H.V. Poor, P. Popovski, T. A. Tsiftsis, Private 5G networks: concepts, architectures, and research landscape, IEEE J. Sel. Top. Signal Process. 16 (1) (2022) 7–25, https://doi.org/10.1109/JSTSP.2021.3137669.
[2] J. George, M.C. Uko, S.C. Ekpo, M. Ijaz, R. Kharel, Q. Wang, H. Ji, Design of a multiband rf slotted-antenna for biosensing applications. 2020 12th International Symposium on Communication Systems, Networks and Digital Signal Processing (CSNDSP), IEEE, 2020, pp. 1–6.
[3] R.N. Tiwari, P. Singh, B.K. Kanaujia, Bandwidth enhancement using modified L-Probe fed slotted patch antenna for WLAN and UMTS applications, Int. J. Microwave Wireless Technol. 11 (3) (2019) 302–312.
[4] R.N. Tiwari, R. Thirumalaiah, V.R. Naidu, G. Sreenivasulu, P. Singh, S. Rajasekaran, Compact dual-Band 4-Port MIMO antenna for 5G-Sub-Sub 6 Ghz/N38/N41/N90 and WLAN frequency bands, AEU-Int. J. Electron. Commun. 171 (2023) 154919.
[5] M. Uko, S. Ekpo, A 23–28 GHz pHEMT MMIC low-Noise amplifier for satellite-Cellular convergence applications, Int. Rev. Aerospace Eng. J. 14 (5) (2021) 1–10.
[6] M. Uko, S. Ekpo, 8–12 GHZ pHEMT MMIC low-Noise amplifier for 5G and fiber-Integrated satellite applications, Int. Rev. Aerospace Eng. (IREASE) 13 (3) (2020) 99, https://doi.org/10.15866/irease.v13i3.17998.
[7] U. Tripathi, Performance evaluation of microstrip patch antenna with circular slots, J. Inst. Eng. (India): Ser. B (2023) 1–15.
[8] S.C. Ekpo, D. George, Impact of noise figure on a satellite link performance, IEEE Commun. Lett. 15 (9) (2011) 977–979, https://doi.org/10.1109/LCOMM.2011.072011.111073.
[9] B.A. Esmail, S. Koziel, High isolation metamaterial-Based dual-Band MIMO antenna for 5G millimeter-Wave applications, AEU-Int. J. Electron. Commun. 158 (2023) 154470.
[10] C.L. Bamy, F.M. Mbango, D.B.O. Konditi, P.M. Mpele, A compact dual-band dolly-shaped antenna with parasitic elements for automotive radar and 5G applications, Heliyon 7 (4) (2021).
[11] X. Tang, Y. Jiao, H. Li, W. Zong, Z. Yao, F. Shan, Y. Li, W. Yue, S. Gao, Ultra-wideband Patch Antenna for Sub-6 GHz 5G Communications. 2019 International Workshop on Electromagnetics: Applications and Student Innovation Competition (iWEM), IEEE, 2019, pp. 1–3.
[12] D. Konhar, A.K. Behera, S.N. Mishra, D. Mishra, A high gain elliptical slot antenna for lower c-band and x-band application, J. King Saud Univ.-Eng. Sci. 34 (2) (2022) 108–115.
[13] Z. Ding, H. Wang, S. Tao, D. Zhang, C. Ma, Y. Zhong, A novel broadband monopole antenna with t-slot, CB-CPW, parasitic stripe and heart-shaped slice for 5g applications, Sensors 20 (24) (2020) 7002.
[14] Z.H. Ma, Y.F. Jiang, L-Shaped slot-loaded stepped-impedance microstrip structure UWB antenna, Micromachines (Basel) 11 (9) (2020) 828.
[15] P.M. Mpele, F.M. Mbango, D.B.O. Konditi, F. Ndagijimana, A novel quadband ultra miniaturized planar antenna with metallic vias and defected ground structure for portable devices, Heliyon 7 (3) (2021).
[16] A. Atif, A. Majid, M. Zahid, Y. Amin, Circular slotted triangular patch antenna for 5.8 GHz ISM band applications, Eng. Proc. 46 (1) (2023) 10.
[17] L. Wang, Microwave imaging and sensing techniques for breast cancer detection, Micromachines (Basel) 14 (7) (2023) 1462.
[18] S. Thakur, R. Mishra, S.K. Soni, P.K. Rao, Crescent-Shaped slot loaded antenna sensor with tri-band notched for cancer detection, Frequenz 76 (9–10) (2022) 569–578.
[19] M.F. Ahmed, M.H. Kabir, A slotted patch antenna design and analysis for detecting breast cancer, ECS J. Solid State Sci. Technol. 12 (4) (2023) 047003.
[20] A.P. Gregory, R.N. Clarke, A review of RF and microwave techniques for dielectric measurements on polar liquids, IEEE Trans. Dielectr. Electr. Insul. 13 (4) (2006) 727–743.

[21] S.C. Ekpo, B. Adebisi, A. Wells, Regulated-element frost beamformer for vehicular multimedia sound enhancement and noise reduction applications, IEEE Access 5 (2017) 27254–27262.
[22] E. Mozaffariahrar, F. Theoleyre, M. Menth, A survey of wi-fi 6: technologies, advances, and challenges, Future Internet 14 (10) (2022) 293.
[23] R.B. Simorangkir, Y. Yang, K.P. Esselle, B.A. Zeb, A method to realize robust flexible electronically tunable antennas using polymer-embedded conductive fabric, IEEE Trans. Antennas Propag. 66 (1) (2017) 50–58.
[24] Y. Zhang, Y. Zhang, D. Li, K. Liu, Y. Fan, Dual-polarized band-notched antenna without extra circuit for 2.4/5 GHz WLAN applications, IEEE Access 7 (2019) 84890–84896.
[25] M. Zada, I.A. Shah, H. Yoo, Integration of sub-6-GHz and mm-wave bands with a large frequency ratio for future 5G MIMO applications, IEEE Access 9 (2021) 11241–11251.
[26] J. Lan, Z. Yu, J. Zhou, W. Hong, An aperture-sharing array for (3.5, 28) GHz terminals with steerable beam in millimeter-wave band, IEEE Trans. Antennas Propag. 68 (5) (2019) 4114–4119.
[27] L. Sun, H. Feng, Y. Li, Z. Zhang, Compact 5G MIMO mobile phone antennas with tightly arranged orthogonal-mode pairs, IEEE Trans. Antennas Propag. 66 (11) (2018) 6364–6369.
[28] Z. Nie, H. Zhai, L. Liu, J. Li, D. Hu, J. Shi, A dual-polarized frequency-reconfigurable low-profile antenna with harmonic suppression for 5G application, IEEE Antennas Wirel. Propag. Lett. 18 (6) (2019) 1228–1232.
[29] K. Xue, D. Yang, C. Guo, H. Zhai, H. Li, Y. Zeng, A dual-polarized filtering base-station antenna with compact size for 5G applications, IEEE Antennas Wirel. Propag. Lett. 19 (8) (2020) 1316–1320.
[30] M. Santosh Kumar, S. Ajit Kumar, S. Rashmi, A. Mohammad, K. Salahuddin, P. Giovanni, High isolated four element MIMO antenna for ISM/LTE/5G (sub-6GHz) applications, IEEE Access 11 (2023) 82946–82959, https://doi.org/10.1109/ACCESS.2023.3301185.

Jeena George was born in Kerala, India, in 1994. She received the B.Tech. degree in Electronics and Communication Engineering from the Cochin University of Science and Technology, Kerala, India in 2016 and the M.Sc. degree in Electronic Engineering from the Manchester Metropolitan University, Manchester, UK in 2018. She is currently working as a Research and Development Engineer at Unifi.id, London. Her current research interest includes radio frequency engineering, biosensing, RFID, RF energy harvesting, multilayer antenna technologies, metamaterials, and 5G communications.

Mfonobong Uko received his B.Eng. degree in Electrical/Electronic Engineering from the University of Uyo, Nigeria and MSc in Communication Engineering from The University of Manchester, UK. He is a PhD candidate in Communication Engineering at the Manchester Metropolitan University, UK. His research interest is adaptive satellite system design; multi-physics design, and modelling of RF, microwave, millimetre-wave, and optical transceivers; internet of things sensors characterisation; multi-objective system engineering; and complex systems optimisation.

Sunday Ekpo obtained the MSc. Degree in Communication Engineering from the University of Manchester, Manchester, UK in September 2008 and proceeded for his PhD degree in Electrical and Electronic Engineering at the same institution. He specialises in highly adaptive satellite system design; multi-physics design, and modelling of RF, microwave, millimetre-wave, and optical transceivers; internet of things sensors characterisation; multi-objective system engineering; and complex systems optimisation. He holds a PGC. in Academic Practice and MA. in Higher Education. Dr Ekpo is a Senior Lecturer in Electrical and Electronic Engineering; leads the Communication and Space Systems Engineering research team at the Manchester Met-University, UK; Chartered Engineer; and Senior Fellow of the Higher Education Academy (UK). He is a member of the Institution of Engineering and Technology, IEEE and the American Institute of Aeronautics and Astronautics.

Fanuel Elias is an accomplished Electrical and Electronics Engineering researcher who received his first-class BEng Degree in Electrical and Electronics Engineering from the Manchester Metropolitan University, UK, in 2023. His award-winning final year project focused on Reconfigurable Wireless WIFI6/ 6E/7/5G Energy Harvesting Design. He is pursuing a PhD in RF Engineering and specialises in Reconfigurable Holographic Multi-Radio Metasurface Rectennas for Ultra-low Power 5G/Wi-Fi 6/6E/7/Halow Applications. He's also a research assistant for the Royal Academy of Engineering, contributing to Premenstrual Dysphoric Disorder (PMDD) sensors. His expertise encompasses RF engineering, including subsystem design, rectifiers, antenna design, and RF transceiver characterisation. His research interests lie in metamaterial and metasurface analysis, specifically emphasising energy harvesting and antenna applications, driving innovation in wireless communication technology.